RSC Advances

REVIEW

View Article Online
View Journal | View Issue

Cite this: *RSC Adv.*, 2026, **16**, 3034

Therapeutic horizons in the development of PROTAC-based EZH2 inhibitors: recent achievements, comparative analysis, and future perspectives

Hamada S. Abulkhair *[ab]

EZH2, a histone methyltransferase and the catalytic subunit of the polycomb repressive complex 2 (PRC2), plays a pivotal role in tumor epigenetics through transcriptional repression of tumor suppressor genes. Despite the clinical success of tazemetostat, classical small-molecule inhibitors face limitations related to incomplete target occupancy, adaptive resistance, and non-catalytic EZH2 functions. These challenges have driven a paradigm shift toward proteolysis-targeting chimeras (PROTACs)—bifunctional molecules that inhibit EZH2 through E3 ligase-mediated ubiquitination and proteasomal degradation. This review discusses the design principles, synthetic approaches, structural diversity, and pharmacological profiles of recently developed VHL-, CRBN-, and cIAP-recruiting EZH2 inhibitors reported in the last five years. Comparative analysis of enzymatic inhibition, cellular cytotoxicity, and degradation kinetics highlights **MS8847 (84)** as a verified degrader (DC_{50} = 34 nM in EOL-1 cells) with concentration- and time-dependent activity, establishing a benchmark for efficient EZH2 elimination. Compounds **P3 (72)** and **P4 (73)** (VHL-based) and **U3i (44)** (CRBN-based) also demonstrated potent dual biochemical and cellular profiles. Recent findings emphasize structure–activity trends, ligase selectivity, and linker optimization as decisive parameters for balancing efficacy and selectivity. Future directions focus on integrating novel ligases, proteome-wide selectivity mapping, and computational modeling to refine degradation efficiency and minimize off-target effects. Collectively, these developments explain a transformative therapeutic horizon where EZH2-targeting PROTACs are dignified to overcome the intrinsic limitations of enzyme inhibition, offering a new era of epigenetic cancer therapy through targeted protein degradation.

Received 12th November 2025
Accepted 22nd December 2025

DOI: 10.1039/d5ra08746e

rsc.li/rsc-advances

[a]*Pharmaceutical Organic Chemistry Department, Faculty of Pharmacy, Al-Azhar University, Nasr City, Cairo 11884, Egypt. E-mail: hamadaorganic@azhar.edu.eg*

[b]*Pharmaceutical Chemistry Department, Faculty of Pharmacy, Horus University-Egypt, International Coastal Road, New Damietta 34518, Egypt. E-mail: habulkhair@horus.edu.eg*

Hamada S. Abulkhair

Hamada S. Abulkhair *obtained his PhD degree in 2010 from Al-Azhar University, Egypt, in the field of Pharmaceutical Organic Chemistry. In 2015, and for three years, he joined Zewail City of Science and Technology where he was promoted to Associate Professor in 2017. The principal research efforts of Professor Abulkhair include the development of small molecule inhibitors of bioactive proteins for the management of cancer. This research combines tools from organic synthesis, structural biology and molecular modeling. Prof. Abulkhair's published articles include sixty-one articles in high-ranked peer-reviewed journals, including European Journal of Medicinal Chemistry, Bioorganic Chemistry, Scientific Reports, RSC Advances, Archiv der Pharmazie, Molecules, New Journal of Chemistry, Journal of Biomolecular Structure & Dynamics, Bioorganic & Medicinal Chemistry, Molecular Diversity, Pharmaceuticals, and Journal of Heterocyclic Chemistry. He's currently serving as an adjunct Professor at the Department of Pharmaceutical Chemistry at Horus University in Egypt since 2018. The Scopus h-index of Prof. Abulkhair is 36. He served as scientific editor in Discover Biotechnology (Springer), and as a reviewer for more than 90 articles in high-ranked international journals as indicated by Clarivate analytics.* ***Research impact****: fifty-eight peer-reviewed publications indexed in Scopus; over 2200 citations from 1130 documents; h-index: 36; collaborated with more than 190 co-authors worldwide (December 2025). SCOPUS: https://www.scopus.com/authid/detail.uri?authorId=57194105398.*

1 Introduction

The dynamic regulation of gene expression through epigenetic mechanisms has emerged as a cornerstone of modern oncology research. Among the key players in this regulatory background is Enhancer of Zeste Homolog 2 (EZH2), a histone methyltransferase that catalyzes the trimethylation of lysine 27 on histone H3 (H3K27me3), leading to transcriptional silencing of tumor suppressor genes.[1,2] EZH2 plays a pivotal role in maintaining cellular identity and proliferation.[3,4] Aberrant EZH2 activity has been implicated in a wide spectrum of malignancies, including lymphomas, prostate cancer, and breast cancer.[5]

The therapeutic relevance of EZH2 was established with the FDA approval of Tazemetostat for the treatment of epithelioid sarcoma and follicular lymphoma.[6] This milestone not only validated EZH2 as a druggable target but also catalyzed a surge in medicinal chemistry efforts to develop more potent, selective, and pharmacokinetically favorable inhibitors. Central to these efforts is the exploration of heterocyclic scaffolds, which offer structural diversity, tunable physicochemical properties, and high binding affinity to the SAM-binding pocket of EZH2.

Structurally, EZH2 contains a conserved SET domain responsible for its methyltransferase activity.[7] Mutations within this domain alter substrate specificity and enhance catalytic efficiency.[8] These structural insights have guided the rational design of inhibitors that exploit the conformational dynamics of the SET domain and its cofactor-binding site. Early inhibitors like tazemetostat are based on pyridone scaffolds, which mimic the natural cofactor *S*-adenosylmethionine (SAM) and competitively inhibit methyltransferase activity. However, recent years have witnessed the emergence of a broader array of heterocyclic frameworks, including thieno[3,2-*d*]pyrimidines,[9] benzofurans, benzo[1,4]oxazines,[10] and indoles,[11] many of which exhibit improved potency, selectivity, and metabolic stability.

In parallel, the advent of proteolysis-targeting chimeras (PROTACs) has introduced a paradigm shift in EZH2-targeted therapy.[12,13] Unlike classical inhibitors, PROTACs induce selective degradation of EZH2 by hijacking the ubiquitin-proteasome system.[13] Several heterocyclic PROTACs have shown superior efficacy compared to traditional inhibitors, particularly in models resistant to catalytic blockade. Fig. 1 provides a multidimensional summary of research trends related to EZH2-targeting therapies including chemistry-oriented journal distribution, the split of research focus into PROTAC- and non-PROTAC-based inhibitors, keyword co-occurrence, and top contributing researchers in this field.[14] Despite these advances, resistance mechanisms, such as compensatory upregulation of EZH2 mutations in the binding pocket, can limit the durability of response. Moreover, the dual role of EZH2 in normal and malignant tissues necessitates a careful balance between efficacy and toxicity.[4,15] These considerations underscore the need for continued innovation in scaffold design, selectivity profiling, and combination strategies.[16–18] Accordingly, a detailed understanding of EZH2 structural features, mutational landscapes, and oncogenic mechanisms is critical for guiding rational design of next-generation inhibitors.

2 EZH2 as a drug target

2.1 Structural biology of EZH2

From a structural perspective, EZH2 is a multidomain enzyme (Fig. 2), but its SET domain serves as the catalytic core responsible for methyltransferase activity.[19] Within this region, *S*-adenosylmethionine (SAM) enables the enzyme to transfer methyl units onto lysine residues of histone substrates.[20] The SET domain features a highly conserved fold that precisely aligns the cofactor and the histone tail, ensuring selective trimethylation.[19] EZH2's catalytic potential, however, depends on assembly into the PRC2 through interactions with EED and SUZ12.[21] These partner proteins stabilize the SET domain and induce conformational changes required for full enzymatic activation.[21] Consequently, the PRC2 complex functions as a coordinated epigenetic regulator rather than a single catalytic entity. In medicinal chemistry, most small-molecule EZH2 inhibitors are designed to target the SAM-binding cavity of the SET domain, thereby reactivating silenced tumor-suppressor genes.[22] These structural characteristics of EZH2 provide the molecular framework within which oncogenic mutations exert their functional consequences.

2.2 Mutation hotspots and their implications

Across several malignancies, mutations in EZH2 are commonly detected most notably in B-cell lymphomas,[23] where they drive tumorigenesis through hyperactivation of methyltransferase function. The most-characterized mutations, Y641,[24,25] A677G,[26] and A687V,[27] reside within or adjacent to the SET catalytic domain. Substitutions at Y641 modify EZH2's substrate specificity,[25] enhancing its capacity to induce trimethylation of H3K27.[26–28] Consequently, the development of EZH2 inhibitors requires molecules that retain equivalent potency against both wild-type and mutant enzymes. The clinical success of Tazemetostat in EZH2-mutant tumors[29] highlights the therapeutic relevance of mutation-responsive drug design strategies. Beyond its mutation-driven catalytic dysregulation, EZH2 exerts versatile oncogenic functions that extend into transcriptional control, chromatin remodeling, and non-canonical signaling pathways in cancer.

2.3 Mechanistic role of EZH2 in carcinogenesis

EZH2 promotes epigenetic gene silencing by catalyzing the trimethylation of H3K27me3.[23] However, when EZH2 is overexpressed, this mechanism becomes pathological, leading to the silencing of tumor suppressor genes, which in turn advances uncontrolled cellular proliferation, resistance to apoptosis, and malignant transformation.[30] In hematologic malignancies such as follicular lymphoma, recurrent EZH2 mutations, especially at Y641, produce enzymes with enhanced catalytic efficiency, thereby sustaining oncogenic transcriptional programs (Fig. 3).[30,31] Similarly, in solid tumors, elevated EZH2 expression is consistently associated with aggressive disease progression and poor clinical outcomes.[32] Collectively, these multifaceted actions establish EZH2 as a fundamental regulator of cancer epigenetics and reaffirm its therapeutic value as a druggable

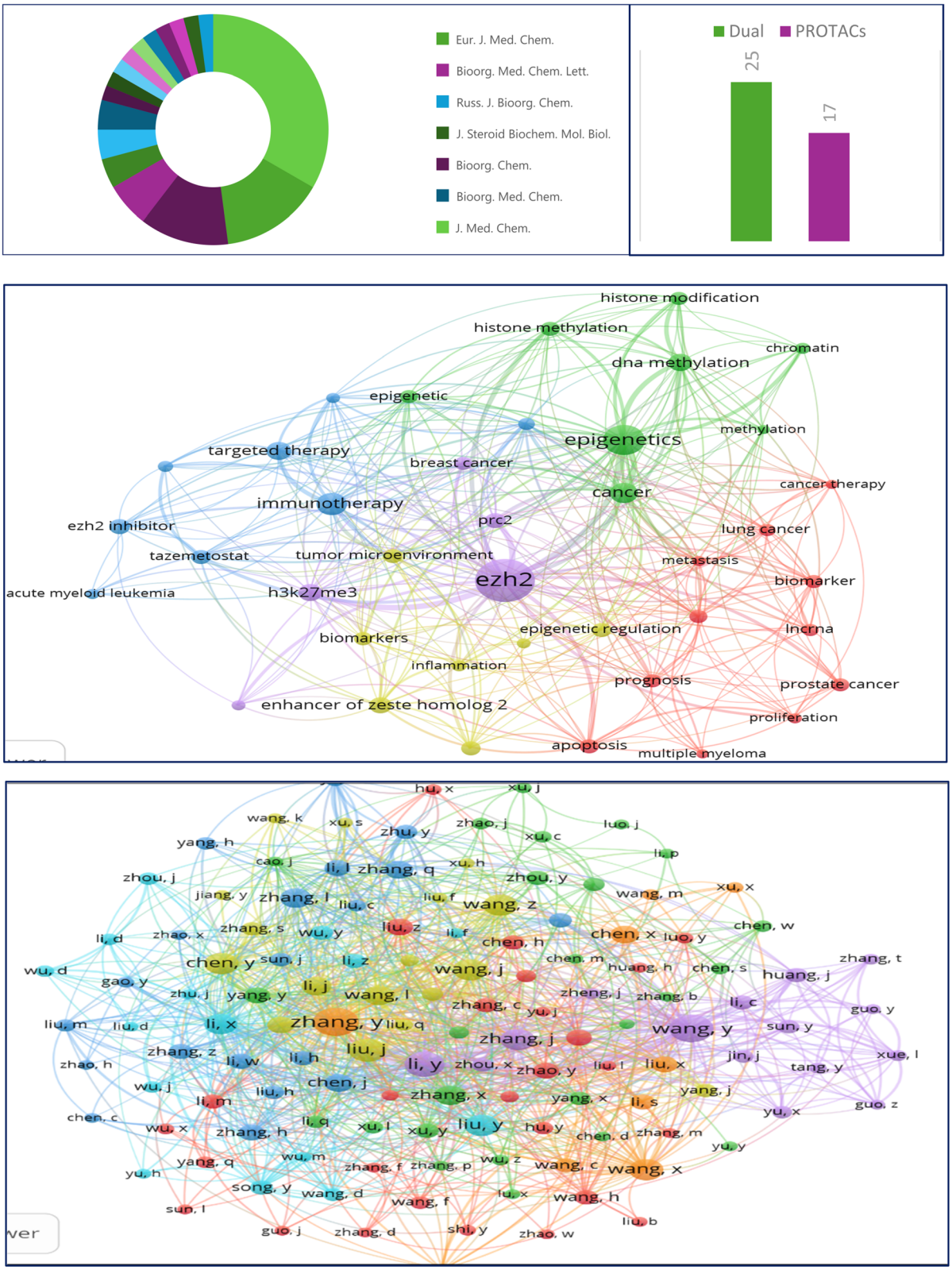

Fig. 1 Global research landscape in EZH2-targeted development (2021–2025). The composite Figure summarizes key scientometric indicators derived from Scopus datasets. A pie chart shows chemistry-oriented journal distribution, where *Journal o Medicinal Chemistry* dominates publication output, underscoring its role as a primary venue for medicinal chemistry-driven EZH2 research (upper left); a bar chart depicts the proportional split of research focus, with 60% dedicated to dual inhibitors, emphasizing the growing interest in multi-target strategies (upper right); a network map illustrates keyword co-occurrence, highlighting "EZH2" as the central node interconnected with terms such as anti-tumor, cancer therapy, epigenetic drug, and PROTAC, reflecting the growing interest in both conventional inhibitors and emerging modalities (middle); author collaboration map reveals a dense cluster of contributors, with prominent nodes like Zhang Y., Liu J., and Chen J., indicating strong collaborative networks driving innovation in EZH2 inhibition (lower). Network map illustrates keyword co-occurrence and author collaboration map have been created using VOSviewer for bibliometric mapping.

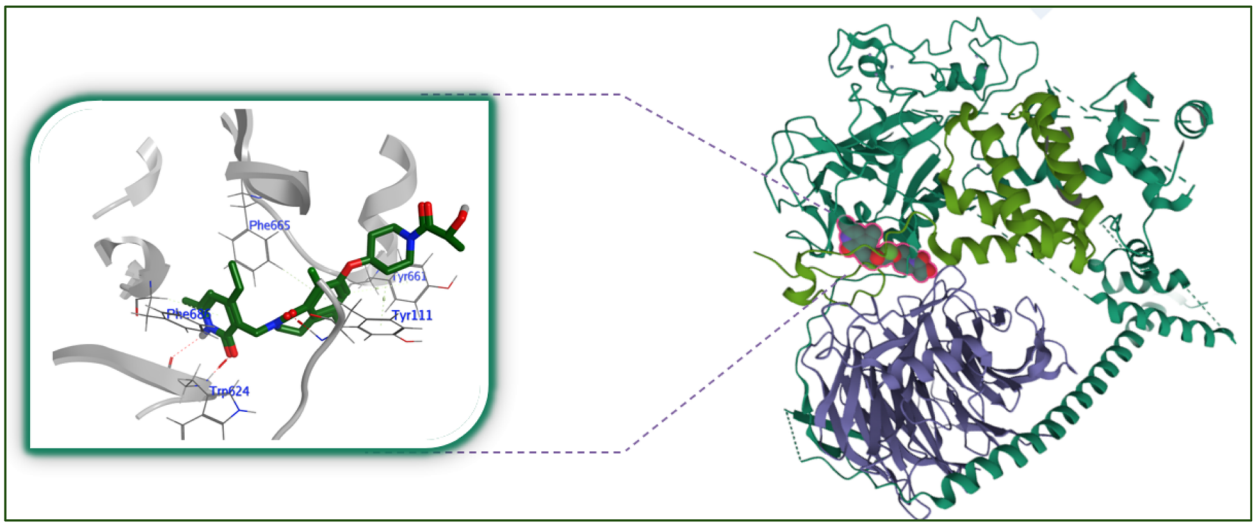

Fig. 2 3D-conformation of PRC2 complex subunits (PDB: 5IJ7, right panel): EZH2 (dark green), EED (light green), and SUZ12 (violet); the co-crystallized ligand 6BN (dark green) bind with the SET domain (left panel).

target. This established role of EZH2 in cancer motivated efforts to translate mechanistic understanding into a targeted chemotherapeutic agent, leading to the development and FDA approval of Tazemetostat.[33]

2.4 FDA approval of tazemetostat and its impact

In January 2020, tazemetostat received accelerated FDA approval as a treatment option of metastatic or locally advanced epithelioid sarcoma.[33,34] This approval was granted based on the overall response rate (ORR) and duration of response observed in pivotal Phase II clinical trials. From a medicinal chemistry standpoint, tazemetostat represents a major milestone in epigenetic cancer therapeutics.[35,36] Mechanistically, it acts as a SAM-competitive inhibitor, effectively blocking EZH2's methyltransferase activity and reactivating transcription of silenced tumor suppressor genes.[37] Importantly, tazemetostat displays high selectivity toward both EZH^{WT} and mutant forms of EZH2.[38] Chemically, tazemetostat is a small, orally bioavailable molecule (molecular weight ≈ 573 Da) featuring a benzamide scaffold, along with morpholine and pyridine rings that optimize binding affinity, solubility, and metabolic stability. The compound demonstrates good oral bioavailability (~33%), extensive tissue distribution, limited CNS penetration, and moderate potential for drug–drug interactions.[37] This regulatory success stimulated the design of next-generation EZH2 inhibitors with enhanced selectivity and pharmacokinetic properties. The SAR optimization leading to tazemetostat involved the identification of **EPZ005687 (2)**, a potent EZH2 inhibitor with a K_i of 24 nM.[39] Structural refinements of **EPZ005687** improved metabolic stability and minimized off-target binding.[40] Another notable analog, **GSK126 (5)**, exhibits >1000-fold selectivity

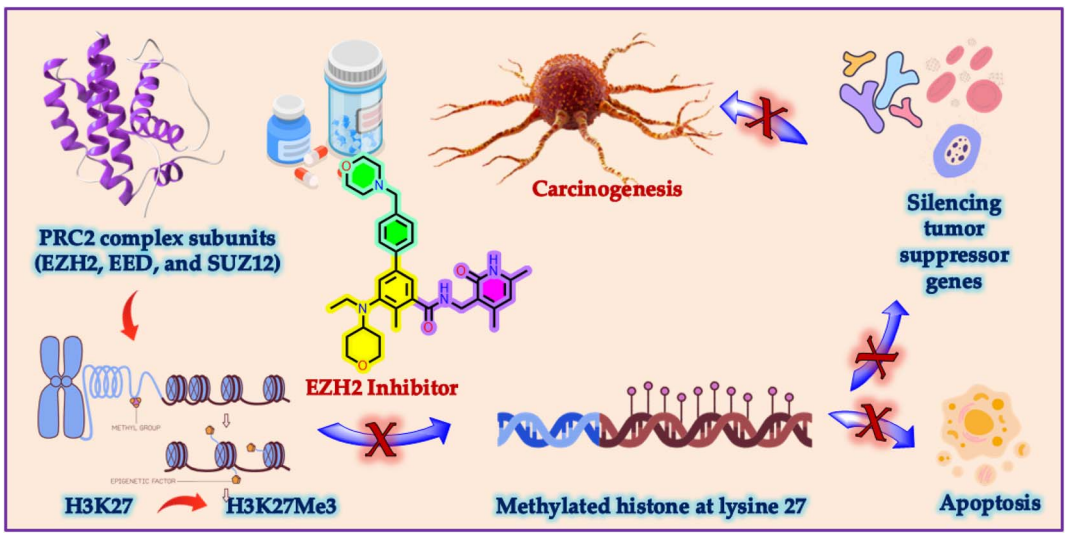

Fig. 3 Mechanism of EZH2 inhibition in cancer therapy.

Table 1 SAR highlights of tazemetostat and representative next-generation EZH2 inhibitors

Compound	Core structure	EZH2 IC_{50}
Tazemetostat	2-Pyridone + phenyl core	2.5 nM
EPZ005687 (2)	2-Pyridone + pyrazolo[3,4-*b*]pyridine	54 nM
EBI-2511 (3)	2-Pyridone + benzofuran scaffold	8.0 nM
IHMT-EZH2-115	2-Pyridone + cyclopropane formamide	26.1 nM ($EZH2^{WT}$); 72.3 nM ($EZH2^{Y641F}$)
GSK126 (5)	2-Pyridone + indole	9.9 nM
HM97662	Unavailable	2.1 nM ($EZH2^{WT}$); 1.4 nM ($EZH2^{Y641F}$)[44]

relative to other human methyltransferases and an IC_{50} of 9.9 nM.[41] Furthermore, **HM97662**, a second-generation dual EZH1/2 inhibitor, was developed to overcome resistance mechanisms observed in advanced and metastatic solid tumors.[42] Table 1 summarizes the SAR highlights of representative EZH2 inhibitors, including **EBI-2511**, a potent and orally bioavailable candidate,[10] and **IHMT-EZH2-115** (4), a selective EZH2 inhibitor designed for the treatment of B-cell lymphomas.[43] Given its clinical relevance, detailed insight into the binding mode of tazemetostat within the EZH2 catalytic domain is critical for understanding its inhibitory effect.

2.5 Binding mode of tazemetostat to EZH2

Several amino acid residues in EZH2 have been identified as critical for inhibitor binding and selectivity of common inhibitors like tazemetostat and **GSK126**.[45] These include Trp624, Arg685, Tyr111, and Tyr661 (Fig. 4).[46–50] The ligand's pyridone carbonyl and amide nitrogen form hydrogen bonds with Trp624's backbone carbonyl oxygen and amide nitrogen, effectively mimicking part of the SAM-binding interaction.[46] Arg685 residue forms part of the hydrophobic and polar binding environment that accommodates the inhibitor. The backbone of the inhibitor interacts with the gating residues in the SET domain loop Tyr111 and Tyr661. Collectively, these residues (especially with Trp624 and Tyr111) form a binding cage in which the inhibitor is held. As tazemetostat mimics SAM-binding cavity, it effectively competes with SAM for the active site of EZH2.[51,52] Mutations in pocket residues can perturb the binding cavity geometry, potentially reduce inhibitor affinity and contribute to resistance.[19,51]

3 Clinical progress and challenges

While structure-based inhibition of EZH2 has proven clinically feasible, emerging challenges related to selectivity, resistance, and durability of response necessitate a broader evaluation of therapeutic limitations. Following the FDA approval of tazemetostat,[53,54] ongoing clinical investigations have expanded the therapeutic scope of EZH2 inhibition to include solid malignancies, such as prostate cancer and various pediatric

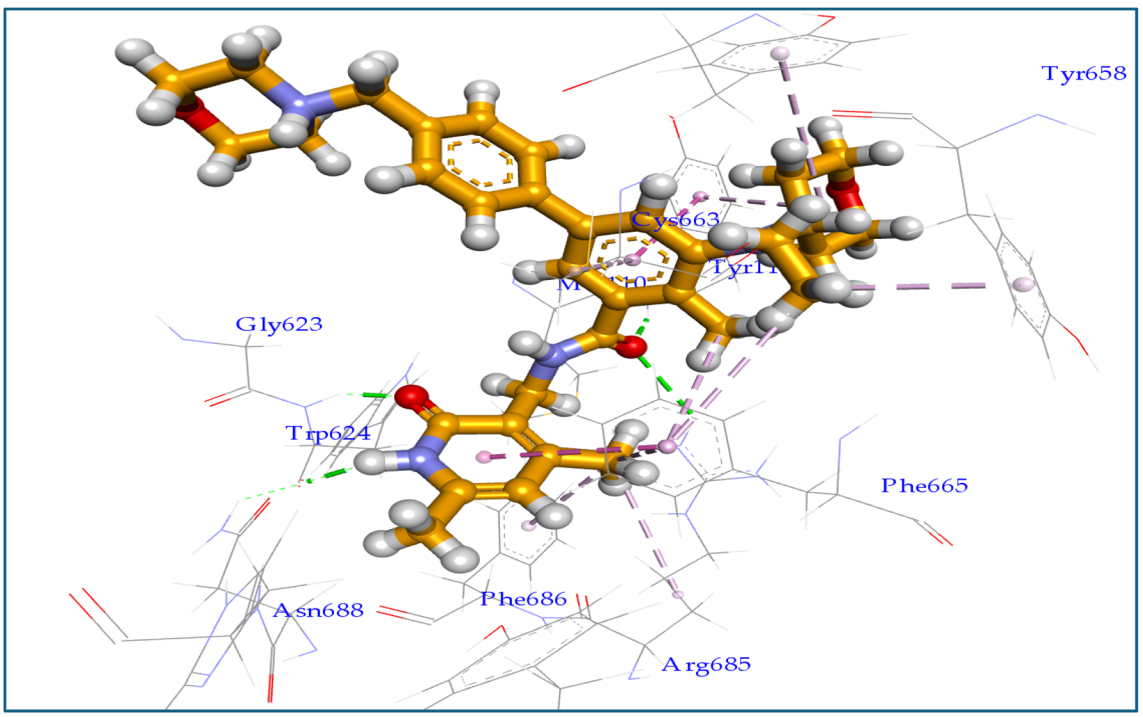

Fig. 4 Binding mode of tazemetostat with EZH2. Visualization of PDB files were conducted by using Dassault Systems BIOVIA Discovery Studio 2017.

tumors.[42,55,56] However, outcomes in prostate cancer have been heterogeneous, with several phase II trials showing limited improvement when EZH2 blockade was combined with androgen receptor-targeted therapies.[57,58] To address the limitations of selective EZH2 inhibition, dual EZH1/EZH2 inhibitors, including **Valemetostat**, **HM97662**, and **Mevrometostat**, are undergoing advanced clinical evaluation.[42,55,59] This dual-targeting approach aims to mitigate compensatory EZH1 activity, thereby enhancing therapeutic breadth and durability.[60] To improve outcomes, combination regimens involving EZH2 inhibitors with BTK inhibitors, chemotherapeutic agents, or other targeted modulators are actively being explored, aiming to enhance efficacy, overcome resistance, and extend clinical benefit across a broader tumor spectrum.[61]

3.1 Selectivity and toxicity

The efficacy of EZH2 inhibitors fundamentally depends on achieving high target selectivity while minimizing off-target interactions.[62,63] Among the approved compounds, tazemetostat exhibits remarkable precision, showing a K_i of 2.50 nM for EZH2, approximately 35-fold higher selectivity over EZH1, and exceeding 4500-fold selectivity across fourteen other methyltransferases.[62] Similarly, **GSK126** demonstrates over 150-fold selectivity for EZH2 *versus* EZH1 and greater than 1000-fold selectivity relative to other methyltransferase enzymes.[64] Despite this strong target preference, EZH1's compensatory activity can diminish overall therapeutic efficacy, which has prompted the development of dual EZH1/EZH2 inhibitors such as valemetostat, designed to address this limitation.[41] Table 2 summarizes the key structural features and selectivity data for representative EZH2 inhibitors. From a safety standpoint, EZH2 inhibitors are generally well tolerated and display a favorable toxicity profile when compared with conventional chemotherapeutics.[65] The most frequent adverse effects are hematologic, including neutropenia (8%), thrombocytopenia (8%), and anemia (6%).[65] These events typically emerge during the first two months of therapy, remain manageable, and are reversible upon dose adjustment or interruption.[65] Non-hematologic effects, such as fatigue, nausea, and reduced appetite, are less common and usually mild.[34,65] Severe or life-threatening toxicities are rare. A systematic meta-analysis encompassing 22 clinical studies ($n = 1002$) reported that treatment-related adverse events (TRAEs) occurred in 86% of patients, with grade ≥3 events in 33% and serious TRAEs in 15%.[66] For tazemetostat specifically, severe neutropenia was observed in roughly 5% of cases, while fatal outcomes remained exceedingly low (0.9%).[34] Long-term safety evaluations, particularly in combination regimens and pediatric populations, are still ongoing. Careful dose optimization and regular clinical monitoring are advised to mitigate risks, especially when EZH2 inhibitors are co-administered with cytotoxic or targeted agents, where the potential for toxicity amplification exists.[67] In summary, while current EZH2 inhibitors display excellent biochemical selectivity and manageable tolerability, next-generation development aims to further refine target discrimination, minimize unintended epigenetic effects, and enhance safety through rational structure optimization and dose-modulation strategies.

3.2 Resistance mechanisms

Malignant tumors can acquire resistance to EZH2 inhibitors through multiple adaptive mechanisms[7,30] (Fig. 5). The principal resistance pathways include the emergence of secondary mutations, activation of prosurvival signaling cascades, uncoupling of differentiation from cell-cycle regulation, epigenetic reprogramming with PRC2 pathway compensation, and reduced responsiveness to next-generation EZH2 or PRC2-targeted agents.[68–70] One major mechanism involves secondary mutations in the EZH2 gene, most often within the SET catalytic domain, which distort the inhibitor-binding pocket.[23] These structural alterations diminish the affinity of compounds such as tazemetostat and **GSK126**, thereby conferring drug resistance. For instance, resistant diffuse large B-cell lymphoma (DLBCL) cell lines have been reported to carry such mutations, which impede inhibitor binding while retaining EZH2's catalytic activity.[71] In addition, constitutive activation of cell-survival

Table 2 Structural formulas, and information on selectivity of the most common EZH2 inhibitors

Comp. name	Information
Tazemetostat	A selective EZH2 inhibitor with K_i of 2.5 nM and IC_{50} of 11.0 nM
CPI-169	Selective; $IC_{50} = 0.24$ nM, and 0.51 nM for $EZH2^{WT}$, $EZH2^{Y641N}$, respectively
PF-06726304	Selective; K_i values of 0.7 nM and 3.0 nM for $EZH2^{WT}$ and $EZH2^{Y641N}$ respectively
Lirametostat	A selective orally effective inhibitor $IC_{50} = 2.0$ nM and EZH1 ($IC_{50} = 52.0$ nM)
UNC1999	A selective orally bioavailable inhibitor of EZH2 (IC_{50} of 2.0 nM)
EPZ011989	A selective orally bioavailable EZH2 inhibitor with K_i of 2.9 nM
GSK343	Selective; IC_{50} of 4.0 nM; 60.0 fold selectivity compared to EZH1
EBI-2511	Selective; orally active EZH2 inhibitor with an IC_{50} of 4.0 nM for $EZH2^{A667G}$
GSK503	A selective EZH2 inhibitor with an IC_{50} value of 8.0 nM
GSK126	A highly selective EZH2 inhibitor with IC_{50} of 9.9 nM, 1000-fold selective for EZH2
EI1	Selective; IC_{50} of 15.0 nM for $EZH2^{WT}$ and 13.0 nM for $EZH2^{Y641F}$
EPZ005687	A potent inhibitor of EZH2 with K_i of 24.0 nM, 50-fold selectivity to EZH2
Gambogenic acid	Selective; binds covalently to Cys668 within the EZH2-SET domain
Valemetostat	A nonselective EZH1/EZH2 dual inhibitor; competitive inhibitor of SAM
JQ-EZ-05	A nonselective and reversible EZH1/EZH2 inhibitor

Fig. 5 Resistance mechanisms to EZH2 targeting anticancer molecules.

pathways, notably PI3K/AKT, MEK/MAPK, and IGF-1R, has been identified as a key compensatory mechanism.[68,72] In DLBCL models, overexpression of PI3KCA, MEK-DD, or IGF-1R alone was sufficient to induce resistance to EZH2 inhibition.[68] Similarly, in SMARCB1-deficient tumors, resistance to tazemetostat has been linked to genetic alterations converging on the RB1/E2F axis.[29,69] Tumor cells may also undergo epigenetic remodeling,[73] decreasing their reliance on EZH2-mediated H3K27 trimethylation as a repressive mechanism and instead activating alternative chromatin-silencing pathways.[69] Interestingly, cross-resistance is not universal: cells resistant to one EZH2 inhibitor (*e.g.*, tazemetostat or GSK126) can remain responsive to others (*e.g.*, UNC1999) or to inhibitors targeting different PRC2 subunits.[68] This observation indicates that resistance frequently arises in a compound-specific manner, suggesting that strategic switching or combination therapy may restore antitumor efficacy. Collectively, these resistance mechanisms, together with selectivity-related concerns, underscore the need for alternative therapeutic strategies such as PROTAC-based EZH2 inhibitors, which aim to eliminate the target protein rather than merely suppress its enzymatic activity.[74–76]

4 Literature survey on PROTAC-based EZH2 inhibitors

Following the FDA-approval of tazemetostat, the past five years have witnessed an exceptional expansion in the chemical entities developed to alter EZH2 function.[77–80] Early generations demonstrated promising suppression of EZH2 methyltransferase activity. However, their therapeutic performance was frequently hampered by incomplete target occupancy and adaptive resistance. These limitations encouraged a paradigm shift from conventional enzymatic inhibition toward targeted protein degradation strategies, particularly the use of PROTACs.[81–83] Unlike classical inhibitors that transiently block the catalytic pocket, PROTACs eliminate the entire EZH2 protein, thereby abolishing both its catalytic and scaffolding functions. This mechanistic advancement has led to the conceptual division of EZH2-targeting agents into two complementary classes: non-PROTAC inhibitors and PROTAC-based degraders. In this context, medicinal chemistry innovations have produced a variety of heterobifunctional EZH2 degraders capable of engaging E3 ubiquitin ligases, such as CRBN and VHL, to trigger ubiquitination and subsequent degradation of EZH2. These degraders provide sustained and comprehensive target suppression, offering therapeutic advantages over reversible inhibition. From a medicinal chemistry perspective, the design of these degraders emphasizes linker optimization. Consequently, EZH2 PROTACs have emerged as dual-purpose molecules, serving as chemical probes for mechanistic studies and as therapeutic leads for next-generation anticancer strategies. In continuation to my recent reviews,[84–90] this review therefore highlights the synthetic strategies, SAR analyses, and pharmacological profiles of recently developed PROTAC-based EZH2 degraders, developed between 2021 and 2025, aiming to provide a comprehensive understanding of their evolution, design principles, and therapeutic promise in targeted cancer therapy.

While previous reviews[7,22,23,30,32,91] have briefly introduced PROTACs as emerging EZH2-targeting tools, the present review shows a comprehensive medicinal chemistry-oriented assessment of EZH2 degraders reported between 2021 and 2025. It systematically compares E3 ligase recruitment (VHL, CRBN, and cIAP), linker design, and SARs while incorporating quantitative degradation parameters (DC_{50}, D_{max}, and time-dependence). Target molecules are discussed in the context of their degradation kinetics and pharmacological efficiency. It integrates standardized biochemical and cytotoxic potency data, systematic SAR analysis, and detailed synthetic strategies across all the reported PROTAC-based EZH2 inhibitors. Furthermore, this review advances a comparative log–log correlation between EZH2 enzymatic and cytotoxic IC_{50} values to assess translational efficiency, an approach not previously reported in the literature. Accordingly, this review outlines a rational background for

designing, optimizing, and validating next-generation EZH2 degraders, thereby filling a critical gap between theoretical PROTAC biology and applied medicinal chemistry.

4.1 Ligase systems in PROTAC-based EZH2 inhibitors

A pivotal determinant of PROTAC efficacy lies in the choice of E3 ubiquitin ligase, the enzyme responsible for recognizing and tagging the target protein for degradation *via* the ubiquitin-proteasome system (UPS). E3 ligases confer substrate specificity by simultaneously binding the PROTAC molecule and the target protein, facilitating the formation of a ternary complex that enables subsequent proteasomal degradation. The human genome encodes over 600×10^3 ligases, but only a limited set has been exploited for PROTAC design of EZH2 degraders (Fig. 6). These include Cereblon (CRBN),[80] von Hippel-Lindau (VHL),[92] MDM2,[93] and cIAP.[93] Among these, CRBN and VHL remain the dominant used ligases in EZH2 PROTAC degraders. CRBN-based PROTACs offer robust cellular activity due to favorable ternary complex formation between the EZH2-binding moiety (often a tazemetostat-derived scaffolds) and the CRBN ligand. Also, VHL-based PROTACs frequently achieve higher selectivity in certain cell types. They are able to recognize hydroxylated proline residues.[94,95] Other ligases, such as MDM2 or cIAP1, have been less explored and often yield limited degradation, highlighting ligase-specific constraints. Comparative analysis suggests that successful EZH2 PROTACs typically require ligases with optimal proximity to the substrate and minimal off-target engagement. This explains the consistent superiority of CRBN and VHL designs in terms of DC_{50} values and degradation efficiency. CRBN was originally identified as the primary target of the immunomodulatory imide-based drugs thalidomide, lenalidomide, and pomalidomide.[96] These imides are now widely used as the ligase-binding moieties in PROTACs. For EZH2, they demonstrated robust target engagement. Recent comparative studies indicated that VHL-based EZH2 PROTACs can achieve efficient degradation of mutant EZH2 variants.[94,95] MDM2 and cIAP ligases have been explored as alternatives in PROTAC research.[93] MDM2 is the principal negative regulator of p53 and has been employed to construct PROTACs in p53-competent cancer models. cIAP-Based ligases mediate ubiquitination through their ring domains and are utilized in the so-called SNIPER (Specific and Non-genetic IAP-dependent Protein Eraser) systems. The limited utility of MDM2 and cIAP as E3 ubiquitin ligases in PROTAC design, including for EZH2 degraders, may be attributed to restricted expression, intrinsic auto-degradation upon ligand binding, mechanistic liabilities, safety concerns, and limited chemical tractability.[97,98] This underperformance of MDM2 and cIAP may be addressed through rational design strategies. The auto-ubiquitination and degradation of the E3 ligase itself can be mitigated by optimizing linker length and rigidity to reduce nonproductive ligase–ligase interactions. Structure-guided exit-vector selection may further stabilize ternary complexes. Additionally, tumor-context-specific deployment represents a viable strategy as MDM2 and cIAP are overexpressed in selected malignancies. Finally, combining MDM2-or cIAP-based EZH2 degraders with agents that stabilize E3 ligase levels or suppress compensatory survival pathways may enhance functional outcomes. Building on these ligase-dependent considerations, numerous PROTAC-based EZH2 degraders have been reported with diverse linkers and warhead designs.

4.2 PROTAC-based EZH2 inhibitors (2021–2025)

Luoting Yu *et al.* designed a series of PROTACs to degrade EZH2 along with other components of the PRC2 complex, *via* the proteasome pathway.[80] The rational design of the target PROTACs was based on the conjugation of selective EZH2 inhibitors (**GSK126** or tazemetostat) to a cereblon (CRBN) E3 ligase-binding ligand (4-hydroxythalidomide) *via* aliphatic linkers of varying lengths (Fig. 7). Two main series, **1–9** and **10–18**, were developed by modifying the piperazinyl or morpholinyl fragments of the inhibitors. The synthetic procedure to achieve **1–9** thalidomide analogs involved the conversion of 4-hydroxyisobenzofuran-1,3-dione into 2-(2,6-dioxopiperidin-3-yl)-4-hydroxyisoindoline-1,3-dione followed by reacting the produced hydroxyisoindoline-1,3-dione with dibromoalkanes under basic conditions. Coupling to EZH2 warhead was achieved by linking **GSK126** to the alkylated thalidomide *via*

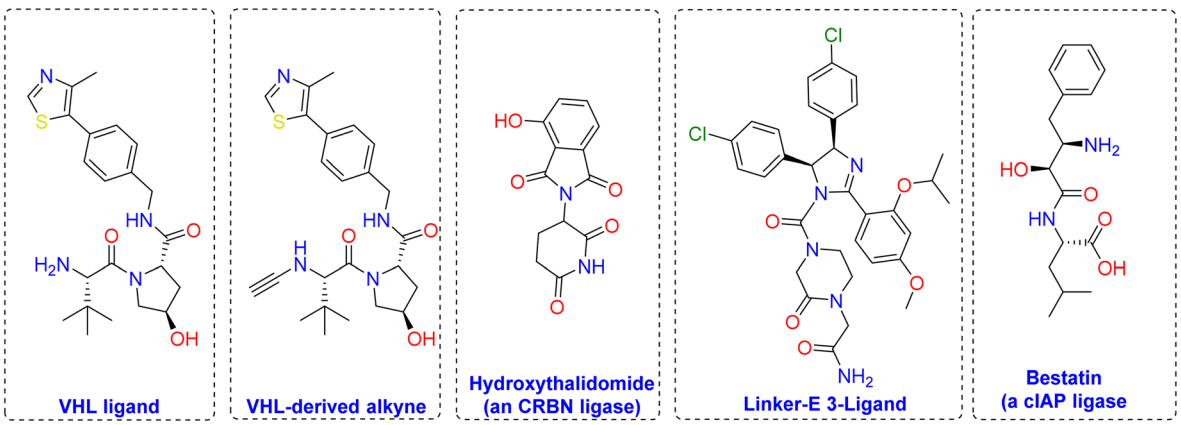

Fig. 6 Common ligases exploited for PROTAC design of EZH2 degraders.

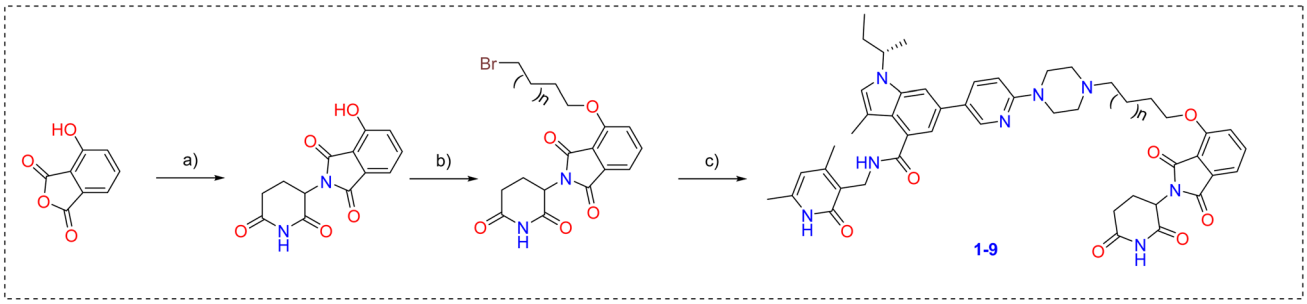

Reagents and Condition

a) 3-Aminopiperidine-2,6-dione, $(CH_3CO)_2O$, 140 °C, 6 h, **71%**;
b) Dibromoalkanes, DMF,*N*,*N*-diisopropylethylamine (DIPEA), 85-100 °C, 3-6 h, **34%-63%**;
c) GS**K**126, $NaHCO_3$, 85-100 °C, 3-8 h, **14%-41%**.

	n =
1	1
2	2
3	3
4	4
5	5
6	6
7	7
8	8
9	9

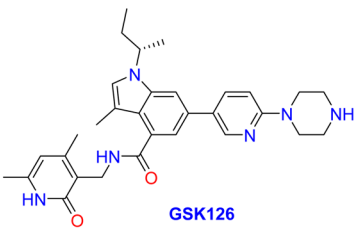

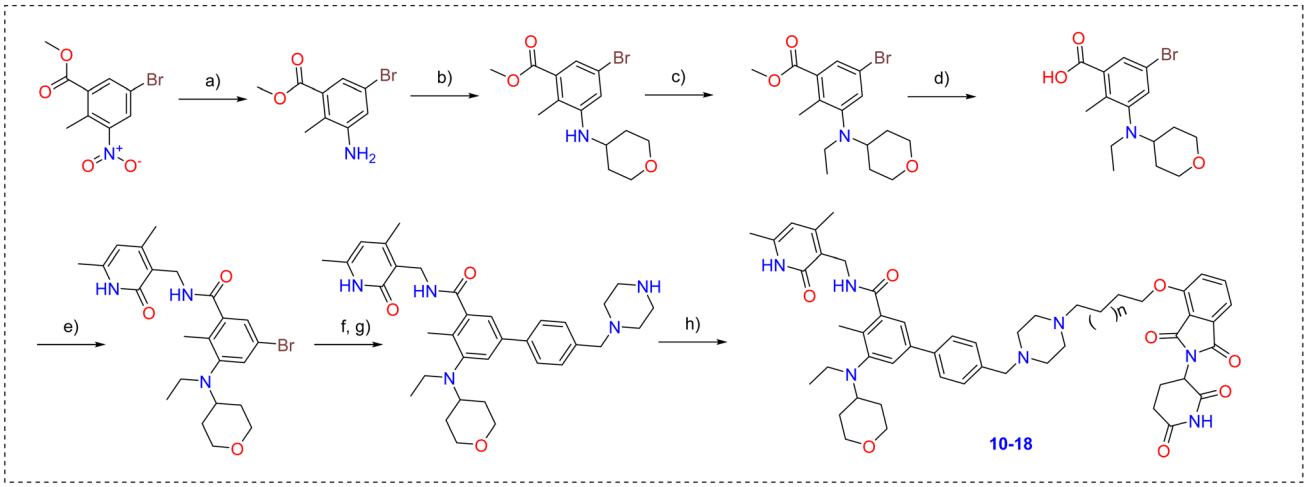

Reagents and Condition

a) Iron powder, NH_4Cl,CH_3OH/H_2O (3:1), 80 °C, **92%**;
b) Tetrahydro-4-pyrone, CH_3COOH, sodium triacetoxyborohydride, $CHCl_3$, rt, 10 h, **57.8%**;
c) Acetaldehyde Anhydrous , 1,2-dichlorethane, CH_3COOH, rt, 10 h, **71%**;
d) 50% NaOH, MeOH,rt, overnight, 2 M HCl, **91.2%**;
e) 1-Hydroxy-7-azabenzotriazole (HOAT), EDCI, DMSO, 45 °C, 20 h, **68%**;
f) K_2CO_3, $Pd(dppf)Cl_2$, 1,4-dioxane/H_2O (4:1), 100 °C, 8 h;
g) TFA, DCM, 25 °C, 1 h, Na_2CO_3 neutralization, **74%**
h) Brominated thalidomide analogs, $NaHCO_3$, DMF, 85-100 °C, 3-8 h, **15%-47%**.

	n =
10	1
11	2
12	3
13	4
14	5
15	6
16	7
17	8
18	9

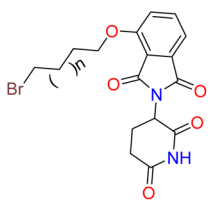

Fig. 7 Adopted synthetic approaches, reagents, and structural formulas of EZH2 inhibitor PROTACs **10–18**.

bimolecular nucleophilic substitution reaction (SN2) at the piperazine nitrogen, forming target PROTACs. For the series **10–18**, a multistep route reaction including reduction, reductive amination, hydrolysis, and Suzuki coupling was used to construct the coupling partner *N*-((4,6-dimethyl-2-oxo-1,2-dihydropyridin-3-yl)methyl)-5-(ethyl(tetrahydro-2*H*-pyran-4-yl) amino)-4-methyl-4′-(piperazin-1-ylmethyl)-[1,1′-biphenyl]-3-carboxamide. SN2 reaction between this last and the brominated thalidomide analogs produced the target PROTACs. The synthesized PROTAC-based EZH2 degraders were evaluated in

Table 3 Biochemical activities of PROTAC-based EZH2 inhibitors **1–9**

	Biochemical activity (IC_{50})			Biochemical activity (IC_{50})	
Cpd. ID	EZH1 (μM)	EZH2 (nM)	Cpd. ID	EZH1 (μM)	EZH2 (nM)
1	0.65	3.70	**10**	0.03	5.50
2	3.53	4.50	**11**	0.06	5.80
3	5.24	3.90	**12**	0.08	4.00
4	4.50	2.70	**13**	0.18	6.30
5	6.70	3.40	**14**	0.21	7.30
6	2.34	15.00	**15**	0.35	16.00
7	>10	17.00	**16**	1.15	144.00
8	7.80	30.00	**17**	0.74	165.00
9	3.61	53.00	**18**	2.52	61.00
GSK126	0.16	2.70	**Tazemetostat**	0.12	3.70

a series of biochemical and cellular assays. These include *in vitro* EZH2 enzymatic inhibition, targeted protein degradation, and mechanism validation. All compounds in both series showed nanomolar activity against EZH2 (Table 3). Notably, compound **13** displayed the highest potency with an IC_{50} value of 2.7 nM) and selectivity over EZH1 (IC_{50} = 179.0 nM).[41] Western blot assays in WSU-DLCL-2 cells showed that **13** induced strong degradation of all PRC2 subunits (EZH2, SUZ12, EED, RbAp48) in a concentration- and time-dependent manner. Compound **13** reduced H3K27me2/3 levels significantly, without affecting unrelated histone modifications, confirming its PRC2-targeting specificity. Co-treatment with CRBN ligand (lenalidomide), proteasome inhibitor (**MG-132**), or NAE inhibitor (**MLN4924**) reversed the degradation effect, confirming CRBN-mediated ubiquitin-proteasomal degradation. qRT-PCR analysis showed that mRNA levels of PRC2 subunits remained unaffected, excluding transcriptional regulation. Compound **13** exhibited strong antiproliferative effects in multiple cancer cell lines, including Pfeiffer (3.69 μM) and prostate (0.21 μM). It significantly reversed both PRC2-dependent transcriptional repression and PRC2-independent transcriptional activation associated with EZH2. Accordingly, compound **13** emerged as the most potent, effectively reducing levels of PRC2 subunits and the H3K27me2/3 histone marks across multiple cancer cell lines.

Shijun Wen *et al.* designed and synthesized novel PROTACs that connect the von Hippel–Lindau (VHL) E3 ligase system to selectively degrade EZH2.[92] In their synthetic strategy, the EZH2 degraders were based on two main pharmacophores (Fig. 8): (i) An EZH2-binding warhead derived from tazemetostat; (ii) A VHL-binding ligand derived from hydroxyproline. These two units were connected *via* alkyl or PEG-based linkers of variable length and flexibility to optimize ternary complex formation and degradation potency. The general synthesis steps included the key modifications on the piperazine ring of tazemetostat analogs, to enable *N*-alkylation or amide coupling with linker units. The VHL ligand was synthesized from (*S*)-*tert*-leucine and protected hydroxyproline, followed by coupling with linkers. The final PROTAC molecules *e.g.*, **YM281 (20)** and **YM181 (21)**, were built *via* amide bond formation between the EZH2 warhead and the VHL-binding fragment using EDC/HOBt or HATU as coupling agents.

Biological evaluation studies included EZH2 and H3K27me3 inhibition, antiproliferative activity, apoptosis, cell cycle effects, and permeability assays. Western blot analysis confirmed that **YM181 (21)** and **YM281 (20)** induced potent, dose-dependent inhibition of EZH2 and a significant reduction in H3K27me3 levels in 22Rv1, SU-DHL-2, SU-DHL-4, and SU-DHL-6 multiple lymphoma cell lines. Compound **25** also showed effective EZH2 degradation in SU-DHL-2 cells, confirming VHL-mediated activity. MTS assay revealed that **YM281 (20)** and **YM620** potently inhibited the proliferation of lymphoma cell lines. These effects were stronger than the parental EZH2 inhibitor tazemetostat, indicating that target degradation outperformed simple enzymatic inhibition (Table S1 in SI). Flow cytometry analysis showed that **YM181 (21)** and **YM281 (20)** induced cell cycle arrest and apoptosis, accompanied by increased cleaved PARP and Caspase-3 and Caspase-3/7 in treated cells and patient-derived lymphoma samples. In Caco-2 assays, **YM181 (21)** and **YM281 (20)** showed lower permeability ($0.043–0.025 \times 10^{-6}$ cm s^{-1}) compared to tazemetostat (1.304×10^{-6} cm s^{-1}), suggesting potential for further optimization of pharmacokinetics.

YM281 (20) and **YM181 (21)** were predicted to engage EZH2 in a binding mode like tazemetostat, occupying the SAM-binding pocket of the EZH2 SET domain. The VHL ligand occupied its canonical binding cleft on the VHL-Elongin B/C complex, confirmed *via* computational modeling. The linker length and geometry were optimized to allow productive ternary complex formation with both EZH2 and VHL. The docking analysis supported that effective degradation was dependent on simultaneous high-affinity binding to both targets and linker orientation that facilitates proximity-induced ubiquitination.[92]

Structure-guided design and optimization of PROTACs yielded a series of EZH2 degraders, among which compound **U3i (44)** emerged as the most potent candidate.[79] Chemical procedure adopted for the synthesis of target compounds included the reaction of pyridin-2-yl-piperazin-1-yl-3-oxoalkanoic acids with monomethyl adipate, followed by reaction with VHL ligand to obtain **26–28** (Fig. 9). Relacing monomethyl adipate with 2-azidoacetic acid, followed by click reaction with corresponding VHL ligand produced **29–35**. Alternatively, compound pyridin-2-yl-piperazin-1-yl-3-oxoalkanoic acids were reacted with 4-pentynoic acid, followed by click reaction with corresponding CRBN

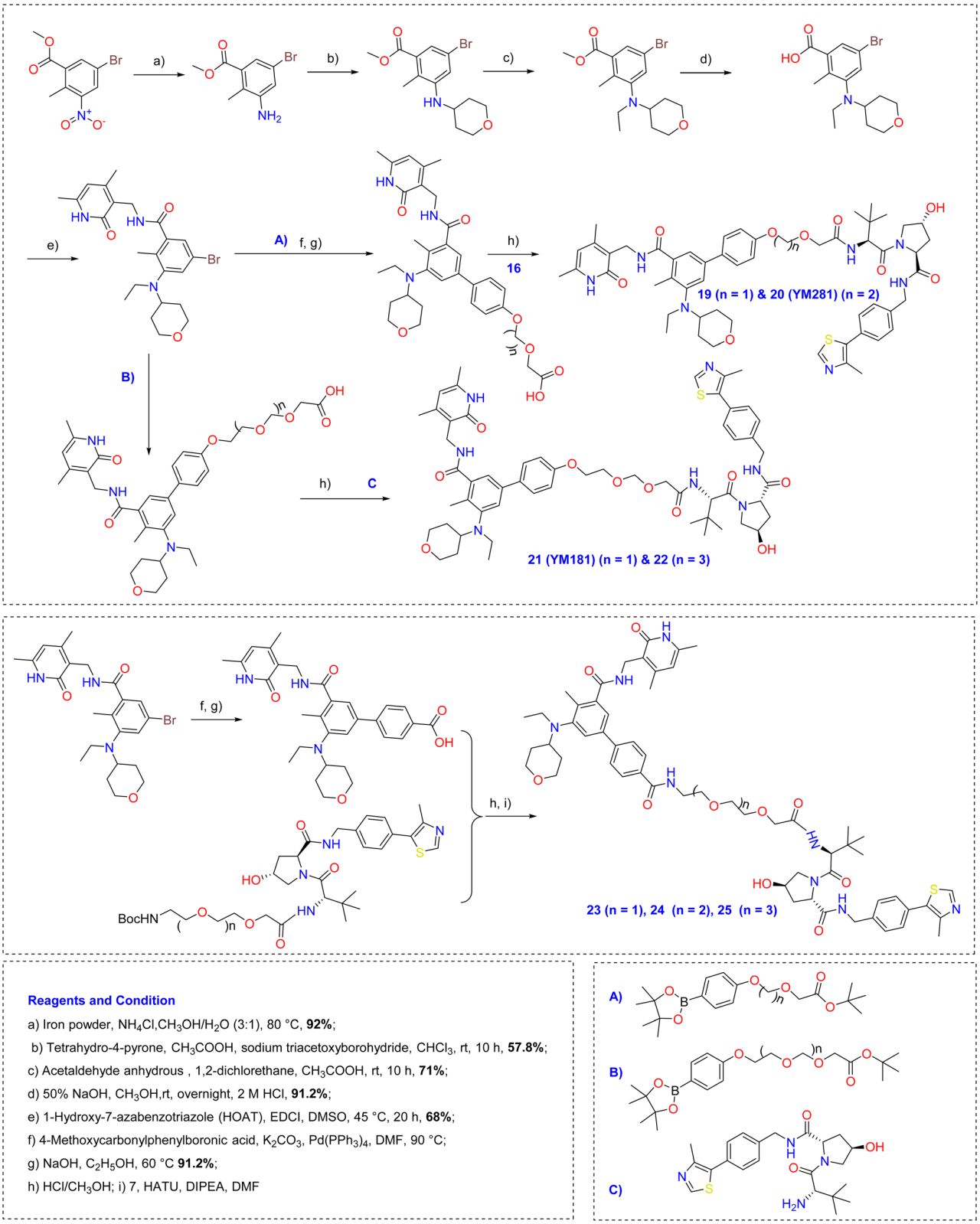

Fig. 8 Adopted synthetic approaches, reagents, and structural formulas of EZH2 inhibitor PROTACs **19–25**.

ligand to obtain **36–45**. Among these, **44** demonstrated high binding affinity to the PRC2 complex with a K_D value of 16.19 nM and exhibited superior antiproliferative activity against EZH2-dependent triple-negative breast cancer cell lines MDA-MB-231 and MDA-MB-468, with IC_{50} values of 0.57 μM and 0.38 μM, respectively. These values represent a 20- to 30-fold

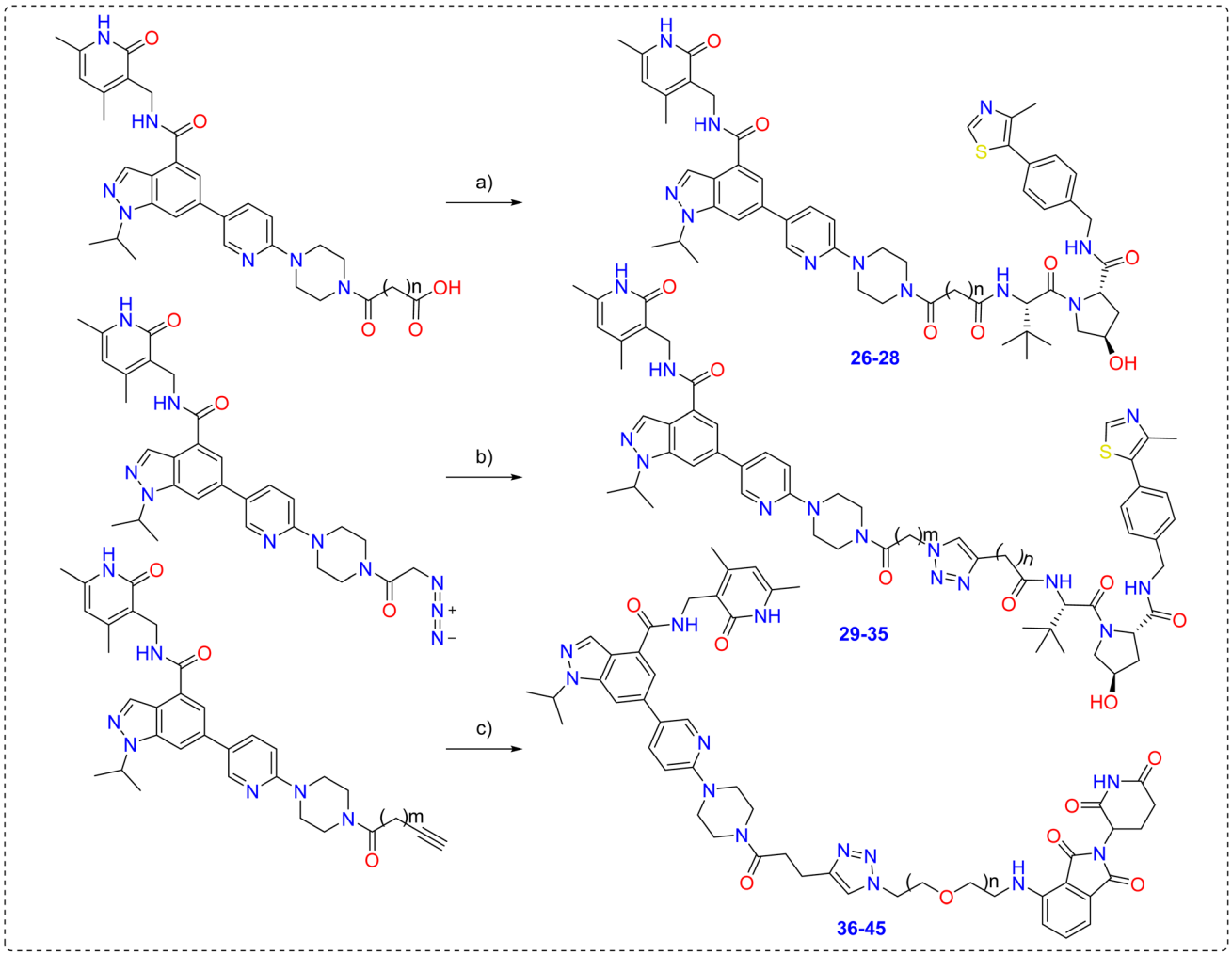

Reagents and Condition

a) VHL ligand, HATU, DIPEA, DCM, rt, 2h; b) Ligand II, $CuSO_4$, NaVic, MeOH/H_2O, rt, 2h.; c) Ligand III, $CuSO_4$, NaVic, MeOH/H_2O, rt, 2h.

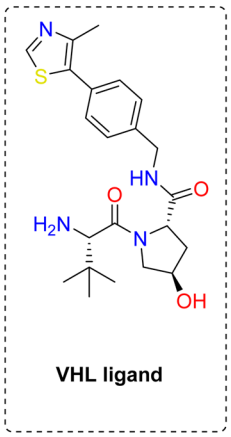

VHL ligand

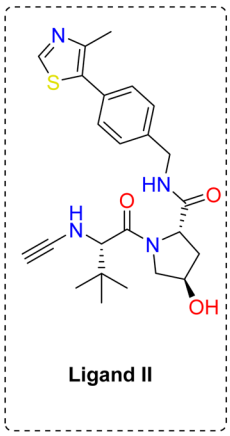

Ligand II

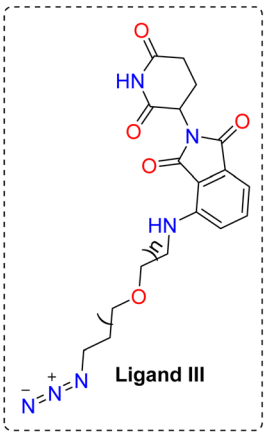

Ligand III

	m	n		m	n
26	-	4	**36**	2	5
27	-	6	**37**	3	5
28	-	7	**38**	4	5
29	1	2	**39**	5	5
30	1	3	**40**	8	5
31	1	4	**41**	8	2
32	4	4	**42**	8	3
33	5	4	**43**	8	4
34	5	5	**44**	8	6
35	5	8	**45**	8	7

Fig. 9 Adopted synthetic approaches, reagents, and structural formulas of EZH2 inhibitor PROTACs **26–45**.

increase in potency compared to the reference inhibitor **GSK126** and over 70-fold compared to tazemetostat. Mechanistic investigations confirmed that **44** induces CRBN- and proteasome-dependent degradation of PRC2 core components (EZH2, SUZ12, and EED), leading to a marked reduction in H3K27me3 and CARM1 levels. Treatment with **44** also triggered mitochondrial dysfunction, as evidenced by decreased membrane potential, and promoted apoptosis *via* upregulation of cleaved

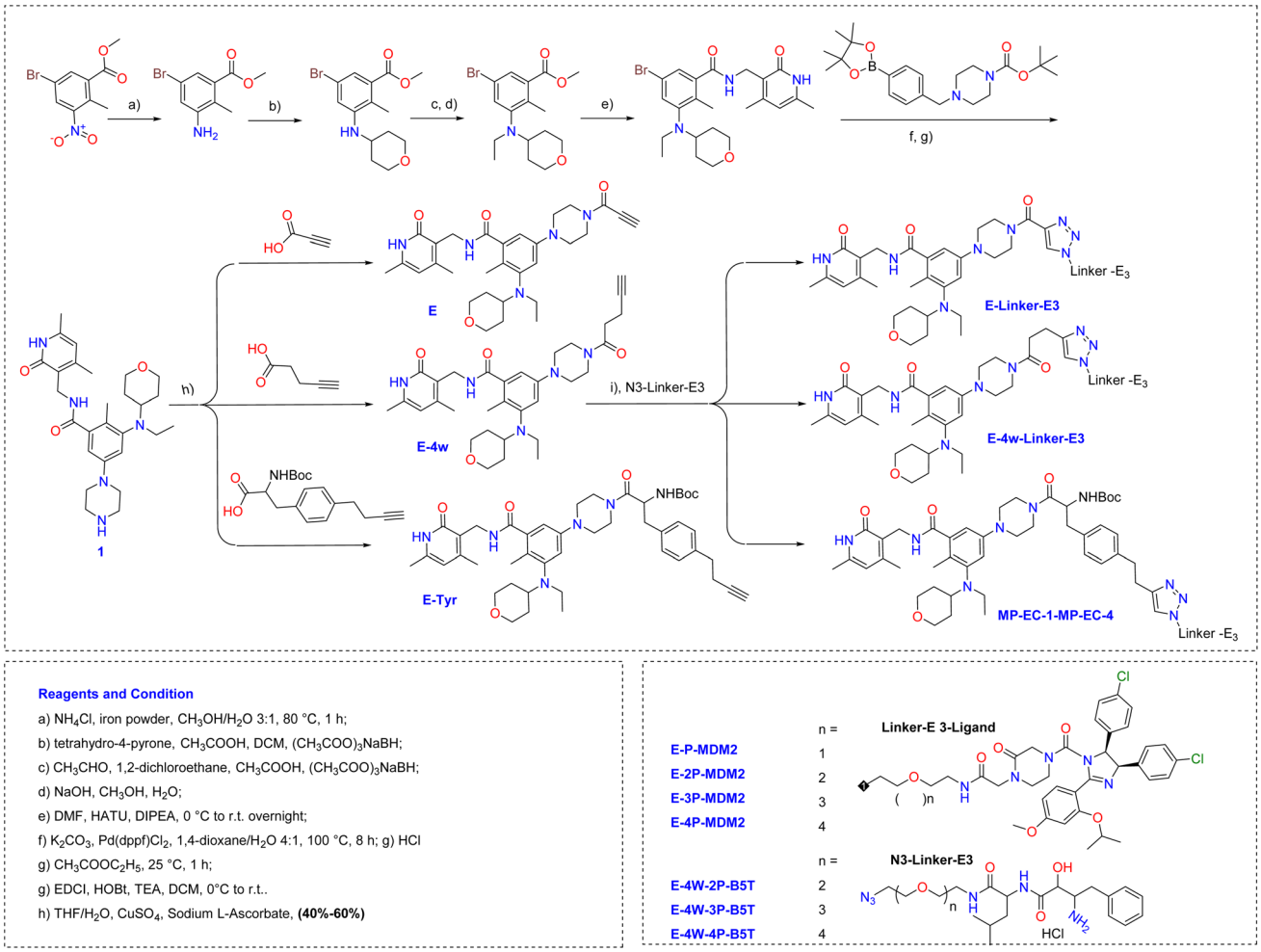

Fig. 10 Adopted synthetic approaches, reagents, and structural formulas of EZH2 inhibitor PROTACs **46–69**. The detailed structures of compounds N3-Linker-E3 and structures of EZH2 PROTACs are provided in Tables S2 and S3 in the SI.

caspase-3 and PARP, alongside downregulation of Bcl-2 and upregulation of Bax. Notably, **44** displayed minimal cytotoxicity in normal human mammary epithelial (MCF-10A), hepatic (LO2), and renal (HK-2) cells. Global proteomic profiling further validated the selectivity of **U3i (44)**, revealing significant downregulation of PRC2 components and enrichment of

Table 4 Cytotoxic activities of PROTAC-based EZH2 inhibitors **46–69**

Cpd. Code	Core structure	E3 ligase ligand	IC_{50} (μM)[b] SU-DHL-6	HBL-1	Cpd. Code	Core structure	E3 ligase ligand	IC_{50} (μM)[b] SU-DHL-6	HBL-1
46	**MP-EC-2**	[a]Thal	>30.00	>30.00	**59**	**E-CH2-V1**	VH 032	21.73	>30.00
47	**MP-EC-3**	Thal	>30.00	>30.00	**60**	**E-5CH2-V1**	VH 032	2.99	6.77
48	**MP-EC-4**	Thal	>30.00	>30.00	**61**	**E-CH2-V2**	VH 032	22.97	>30.00
49	**E-2P-T**	Thal	>30.00	>30.00	**62**	**E-3CH2-V2**	VH 032	>30.00	>30.00
50	**E-3P-T**	Thal	18.21	>30.00	**63**	**E-5CH2-V2**	VH 032	>30.00	>30.00
51	**E-4P-T**	Thal	13.74	>30.00	**64**	**E-7CH2-V2**	VH 032	16.2	>30.00
52	**E-5P-T**	Thal	>30.00	18.32	**65**	**E-4W-7CH2-V2**	VH 032	>30.00	>30.00
53	**E-CH2-B4**	[b]Best	6.64	24.74	**66**	**E-P-MDM2**	MDM2 ligand 2	24.53	>30.00
54	**E-4W-CH2-B4**	Best	10.38	10.26	**67**	**E-2P-MDM2**	MDM2 ligand 2	6.22	>30.00
55	**E-4W-3CH2-B4**	Best	14.33	10.81	**68**	**E-3P-MDM2**	MDM2 ligand 2	3.39	17.48
56	**E-4W-2P-B5T**	Best	15.35	>30.00	**69**	**E-4P-MDM2**	MDM2 ligand 2	3.63	8.74
57	**E-4W-3P-B5T**	Best	10.22	10.17		**Tazemetostat**	—	21.95	>30.00
58	**E-4W-4P-B5T**	Best	14.48	8.35					

[a] Thal. = Thalidomide. [b] Best. = Bestatin.

apoptosis-related pathways. Collectively, these findings establish **U3i (44)** as a promising precision-targeted degrader of EZH2 with potent and selective antitumor activity in TNBC models. SAR analysis of linker length for **36–45** revealed that increasing the PEG linker length from **36** to **40** improved the anti-proliferative potency. Further optimization of the PEG linker length led to the most active compound **44**.

Several PROTACs were synthesized by combining tazemetostat with VHL, CRBN, MDM2, and cIAP E3 ligase ligands.[93] To synthesize the target EZH2 inhibitor ligands, compound 1 was first obtained in 7 steps (Fig. 10): (i) reduction of methyl 3-bromo-5-nitrobenzoate with iron powder and ammonium chloride to obtain methyl 3-amino-5-bromo-2-methylbenzoate; (ii) reductive amination of the produced ester with tetrahydro-4-pyrone; (iii) alkaline hydrolysis of the ester group in the resulting methyl 3-((tetrahydro-2*H*-pyran-4-yl)amino)benzoate using NaOH to obtain; (iv) coupling of 5-bromo-3-(ethyl(tetrahydro-2*H*-pyran-4-yl)amino)-2-methylbenzoic acid with 3-(aminomethyl)-4,6-dimethylpyridin-2(1*H*)-one using HATU and DIPEA to form the corresponding amide derivative; (v) suzuki coupling of the resulting intermediate with *tert*-butyl 4-(4-(4,4,5,5-tetramethyl-1,3,2-dioxaborolan-2-yl)benzyl) piperazine-1-carboxylate; (vi) removal of the protecting group to get compound **1**; (vii) condensation of **1** was with propionic acid amide to get intermediate. A set of copper-promoted click reactions was then adopted to combine azides and alkynes two intermediates (**E** and **N3-nP-MDM2**) and directly assembles a new small PROTAC molecule (**E-nP-MDM2**). A set of twenty-four EZH2 PROTACs were synthesized by combining the EZH2 ligands with different E3 ligase ligands (CRBN, VHL, cIAP, MDM2) using copper-catalyzed click chemistry. For instance, **E-nP-MDM2** PROTACs were obtained by condensing **E** with the MDM2 ligand **N3-nP-MDM2** while **E-4W-nP-B5** PROTACs were

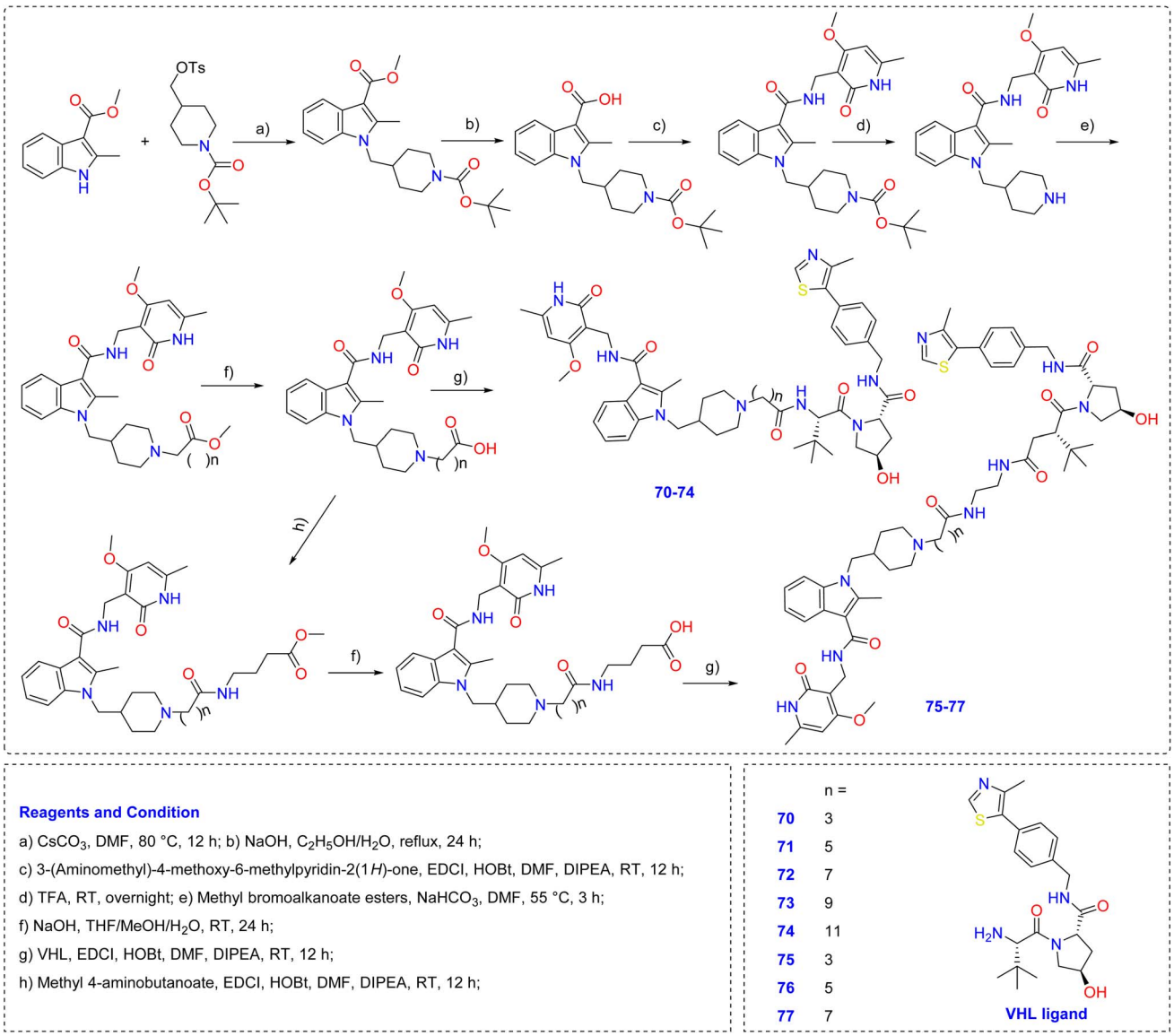

Fig. 11 Adopted synthetic approaches, reagents, and structural formulas of EZH2 inhibitor PROTACs **70–77**.

obtained by condensing **E-4W** with the cIAP ligand **N3-nP-B5** (Tables S2 and S3 in SI).

Among the **E3** ligand-based PROTACs synthesized, the compound **E-4W-3P-B5T (57)** showed the most potent degradation effects on EZH2. **E-4W-3P-B5T (57)** was able to degrade EZH2 at 10.00 μM and 30.00 μM concentrations in the SU-DHL-6 cell line (Table 4). Other **E3** ligand-based PROTACs like **E-CH2-B4** had fewer degradation effects on EZH2 compared to **E-4W-3P-B5T (57)**. **E-3P-MDM2** induces apoptotic cell death in SU-DHL-6 *via* mitochondrial pathway.

A modular synthetic strategy was employed to construct the series of PROTACs targeting EZH2 (**P1–P8**) by conjugating a known EZH2 inhibitor (**CPI-169**) to a VHL E3 ligase ligand through alkyl or amide linkers of varying lengths.[99] A methyl indole ester was alkylated with a Boc-protected piperidine-based tosylate (*tert*-butyl 4-((tosyloxy)methyl)piperidine-1-carboxylate) under basic conditions, yielding the intermediate methyl 1-((1′-(*tert*-butoxycarbonyl)piperidin-4-yl)methyl)-2-methyl-1*H*-indole-3-carboxylate. Ester hydrolysis followed by condensation with 3-(aminomethyl)-4-methoxy-6-methylpyridin-2(1*H*)-one and deprotection furnished *N*-((4-methoxy-6-methyl-2-oxo-1,2-dihydropyridin-3-yl)methyl)-2-methyl-1-(piperidin-4-ylmethyl)-1*H*-indole-3-carboxamide (Fig. 11). This last was treated with methyl bromoalkanoate esters with varying length (C3–C11) followed by saponification produced a set of piperidin-1-yl)-linked carboxylic acid intermediates, depending on linker length. The final step includes PROTAC formation by condensing the produced acids with pre-synthesized VHL ligand[92] to get the final PROTAC degraders **70–74**. Biological activity assessments included EZH2 inhibition, cytotoxicity, apoptosis and cell cycle arrest under the effect of designed PRPTACs. Compounds **72** and **75** with seven- and three-carbon linkers, exhibited the strongest EZH2 inhibition with IC_{50} values below 3.90 nM (Table 5), outperforming the other compounds (IC_{50} values range 4.10 nM-11.00 nM). The PROTAC-based inhibitor with nine-carbon linker **P4 (73)** induced dose- and time-dependent degradation of EZH2 protein in MDA-MB-231, with more than 80% inhibition at 20.00 μM. Cytotoxicity was evaluated against a panel of five cancer cell lines, including breast cancer and lymphoma. **P4 (73)** demonstrated potent anti-proliferative activity in MDA-MB-468 (IC_{50} = 1.40 μM) and MDA-MB-231 (IC_{50} = 4.48 μM), surpassing SAHA while **P3 (72)** and **P5 (74)** showed milder activity. Flow cytometry analysis revealed that **P4 (73)** induced apoptosis in MDA-MB-231 cells with a total apoptosis rate rising to 35.50%. Western blot confirmed upregulation of cleaved PARP and caspases 3, 7, and 8 in lymphoma cells treated with **P4 (73)**. The same PROTAC derivative triggered G0/G1 cell cycle arrest, raising G0/G1 cellular contents in MDA-MB-231 to 77.70%. Molecular docking experiments on the crystal structure of EZH2 complexed with **GSK-126** (PDB ID: 5WG6) revealed the ability of **P4 (73)** to adopt a binding pose like that of **GSK-126** and to occupy the SET domain pocket. The pyridone moiety of **P4 (73)** formed a key hydrogen bond with Trp624, stabilizing the complex. The VHL ligand formed additional hydrogen bonds with Tyr661, Lys660, and Asp37, supporting dual engagement with EZH2 and VHL.[99]

Considering the structure of the FDA-approved EZH2 inhibitor tazemetostat, Velez *et al.* designed a set of PROTAC degraders recruiting the E3 ligase von Hippel-Lindau (VHL).[100] A propionic acid functionality was introduced onto the EPZ-6438 piperazine ring to enable linker attachment. Intermediates bearing alkyl chains of varying lengths (4–10 carbon linkers) were synthesized, followed by amide coupling to VHL-1-containing modules *via* EDCI/HOAt-mediated condensation (Fig. 12). The final series (**2–8**) was obtained in moderate yield range (19–60%). The optimal inhibitor, **MS8847 (84)**, possessed a 10 C linker, which conferred complete degradation at sub-micromolar concentrations. Negative controls were prepared by (i) methylating tazemetostat amide groups to prevent EZH2 binding or (ii) using a stereoisomer of the VHL ligand to eliminate E3 binding. Linker length SAR analysis revealed that carbon linker length 4–6 failed to degrade EZH2, while carbon linker length 7–8 achieved partial loss, and carbon linker length above 9 units induced robust degradation. **MS8847 (84)** degraded EZH2 in EOL-1 cells with DC_{50} 34.0 nM. Activity was both concentration- and time-dependent, with maximal effect at 24 h. Mechanistic studies showed degradation required both EZH2 and VHL binding, as well as neddylation, and could be rescued by competition with parent inhibitor or free VHL ligand. Selectivity profiling confirmed minimal off-target

Table 5 Biochemical and cellular activities of PROTAC-based EZH2 inhibitors **70–77**

	Cytotoxic activity (IC_{50} μM)					Enzyme assay
Cpd. Code	Pfeiffer	MDA-MB-231	MDA-MB-468	MCF-7	T47D	EZH2 IC_{50} (nM)
70	>50.00	>50.00	>50.00	>50.00	>50.00	—
71	>50.00	>50.00	>50.00	>50.00	>50.00	—
P3 (72)	23.09	29.24	32.27	39.07	>50.00	<3.90
P4 (73)	2.05	4.48	1.40	4.15	6.85	5.40
74	8.50	10.81	4.79	10.75	4.89	11.00
75	>50.00	>50.00	>50.00	>50.00	>50.00	<3.90
76	>50.00	>50.00	>50.00	>50.00	>50.00	4.40
77	>50.00	>50.00	>50.00	>50.00	>50.00	4.10
Tazemetostat	0.13	>50.00	>50.00	>50.00	>50.00	1.10
CPI-169	0.65	>50.00	>50.00	>50.00	>50.00	<3.90
SAHA	—	3.59	5.89	3.15	3.15	—

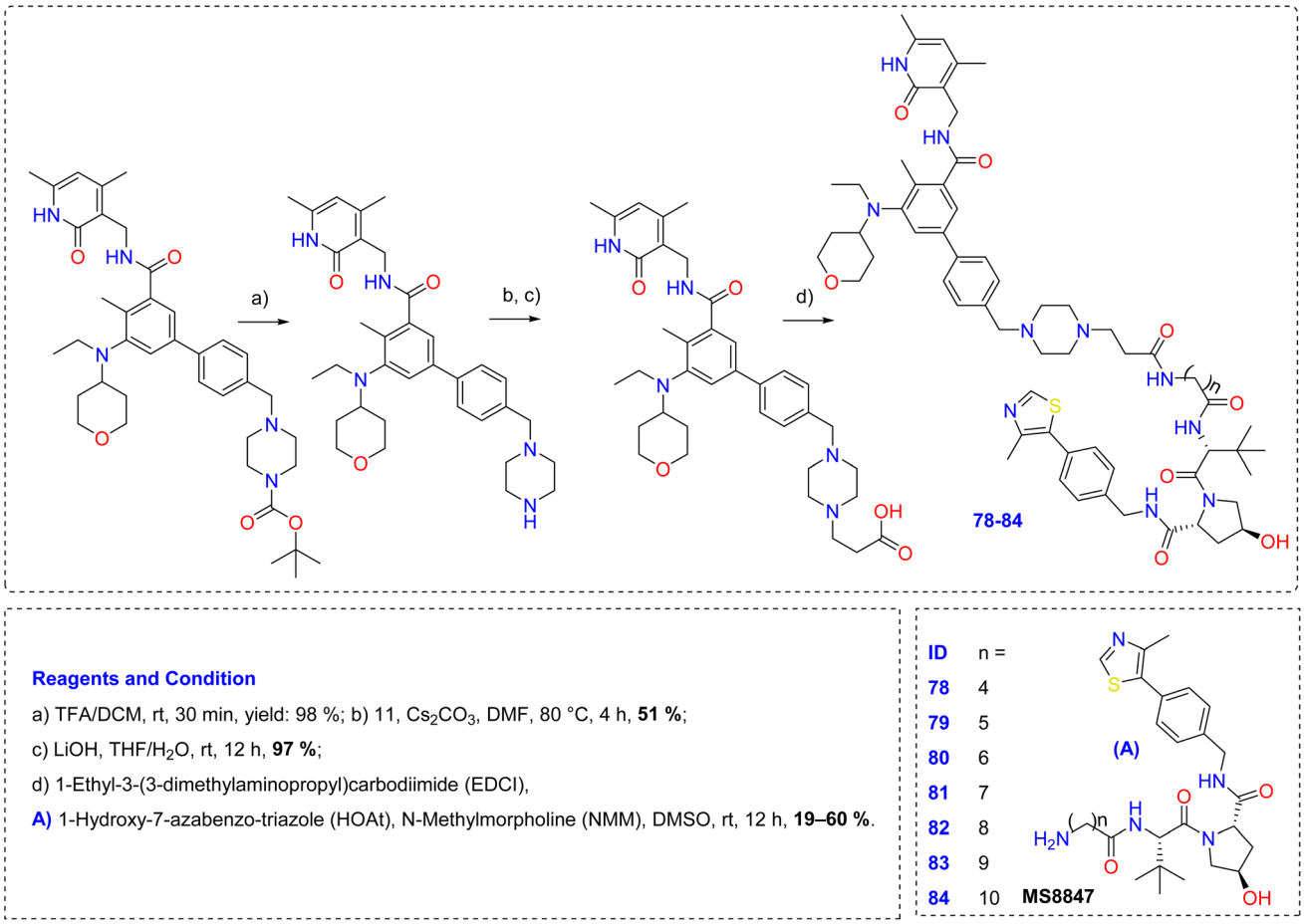

Fig. 12 Adopted synthetic approaches, reagents, and structural formulas of EZH2 inhibitor PROTACs 78–84.

activity against twenty other methyltransferases and no degradation of EZH1.

In comparative assays, **MS8847 (84)** outperformed previously reported PROTACs YM281 (20), U3i (44), E7 (13) in EOL-1. In TNBC lines BT549 and MDA-MB-468, **MS8847 (84)** degraded both cells with IC_{50} values of 1.45 μM and 0.45, whereas tazemetostat had no effect, indicating that the growth of these cells is dependent on EZH2. In RS4 cells, **MS8847 (84)** induced EZH2 degradation at both 0.1 and 0.3 μM and inhibited cell growth with an IC_{50} of 0.41 μM. In a 3D BT549 spheroid model, **MS8847 (84)** significantly reduced tumor size and viability. Docking simulations into the EZH2 active site showed the tazemetostat pyridone scaffold forming conserved hydrogen bonds with residues in the SAM-binding pocket, while the VHL ligand bound its cognate hydrophobic cleft, enabling a productive ternary complex. The linker adopted an extended conformation bridging the two proteins without steric hindrance. Predicted interactions rationalized the superior degradation efficiency of the 10-carbon linker over shorter analogs, as it permitted optimal spatial alignment for ubiquitination. Following a single 50 mg kg^{-1} IP dose in mice, **MS8847 (84)** reached a C_{max} of 3.9 μM at 4 h and maintained >1 μM plasma levels for ~9 h without observable toxicity, indicating favorable bioavailability for efficacy studies.

5 Pharmacological profiles and comparative analysis

A comparative analysis of recently developed EZH2-targeted PROTACs reveals notable advances in potency, degradation efficiency, and cellular activity. Three derivatives exhibit nanomolar inhibition concentrations of EZH2 catalytic activity, with all compounds demonstrating good cytotoxicity profiles. The evaluated candidates employ distinct E3 ligases VHL, CRBN, and cIAP, to trigger ubiquitination and proteasomal degradation of EZH2. Pharmacological assessment across biochemical and cellular assays underscores how ligase selection, linker geometry, and warhead identity collectively shape degradation efficiency and anticancer potential.

5.1 Successful PROTAC design principles

Analysis of PROTAC-based EZH2 degraders in this report demonstrates that productive ternary complex formation, on one hand, is the dominant determinant of degradation efficiency. This is exemplified by **YM281 (20)** which achieves a submicromolar DC_{50} value (34.0 nM).[100] Similarly, **U3i (44)** exhibits efficient EZH2 depletion in lymphoma models ($EZH2^{WT} = 16.19$ nM), confirming that pyridone warheads is compatible with

degradation-oriented design.[79] On the other hand, early designs that preserved strong EZH2 inhibition but lacked favorable exit vector orientation failed to induce robust degradation, underscoring that warhead retention alone is insufficient. Collectively, these examples validate linker geometry, exit vector positioning, and E3 ligase compatibility as decisive parameters in EZH2 PROTAC success.

5.2 Trends by E3 ubiquitin ligase

Compounds such as **YM281 (20)**, **YM181 (21)**, **P3 (72)**, **P4 (73)**, and **MS8847 (84)** are VHL-engaging PROTACs. They show a broad potency range, from low-nanomolar to submicromolar EZH2 IC_{50} values (*e.g.*, **P3 (72)** = 3.9 nM; **P4 (73)** = 5.4 nM; **YM181 (21)** ≈ 0.50 μM). While some compounds display cell-line selectivity such as **P3 (72)**, which is active in lymphoma cells, others exhibit broader antiproliferative activity **P4 (73)**, **MS8847 (84)**. Formation of a productive ternary complex appears critical for high inhibition efficiency, with linker optimization determining whether EZH2 is efficiently polyubiquitinated or merely bound. Among all VHL-based designs, **MS8847 (84)** represents a validated degrader with quantitative degradation kinetics. It induces potent and selective EZH2 degradation in EOL-1 leukemia cells in a concentration- and time-dependent manner, with a DC_{50} of 34.0 nM and maximal effect observed at 24 h. This pharmacodynamic profile strongly supports a true proteasome-mediated degradation mechanism, beyond enzymatic inhibition. In addition to its submicromolar antiproliferative activity in MV4-11 (0.19 μM) and MDA-MB-468 (0.45 μM) cells, **MS8847 (84)** demonstrates that optimized VHL recruitment and linker orientation can achieve deep, durable EZH2 knockdown.

CRBN-Recruiting PROTACs such as **U3i (44)** and **E7 (13)** utilize thalidomide-like ligands. **U3i (44)** displays potent EZH2 inhibition (IC_{50} = 16.19 nM) and strong antiproliferative activity in breast cancer lines (MDA-MB-231 = 0.57 μM; MDA-MB-468 = 0.38 μM), suggesting efficient ternary complex formation and proteasomal degradation. **E7 (13)**, in contrast, shows weak biochemical potency (EZH2 IC_{50} = 6.30 μM) but notable cytotoxicity (PC3 = 0.21 μM). This discrepancy could indicate cell-specific degradation efficacy requiring mechanistic clarification through DC_{50}/D_{max} assays and proteasome inhibition controls. The cIAP-based derivative **E-4W-3P-B5T (57)** showed modest cytotoxicity (SU-DHL-6 = 10.22 μM; HBL-1 = 10.17 μM) without reported EZH2 IC_{50}. While preliminary, it underscores the potential of non-classical ligases to provide complementary degradation profiles when optimized.

5.3 Trends by linker length, rigidity and warhead considerations

Comparative evaluation of EZH2 PROTACs reveals a narrow optimal range for linker design. For example, **P3 (72)** and **P4 (73)**, two closely related VHL-based EZH2 degraders differing mainly in linker length and flexibility, display markedly different degradation efficiencies.[99] **P4 (73)**, which incorporates a slightly extended and more conformationally flexible linker, achieves superior EZH2 inhibition and cellular activity, whereas **P3 (72)** exhibits decreased degradation regardless of comparable biochemical properties. Similarly, in **YM281 (20)** optimization series, excessive linker rigidity resulted in reduced degradation efficiency,[92] likely due to suboptimal ternary complex dynamics. These observations confirm that minor modifications in the linker length can significantly affect biological activity, validating the emphasis on linker fine-tuning in PROTAC-based EZH2 design. Warhead selection as well governs target affinity and specificity. High-affinity EZH2 inhibitors often translate into more effective PROTACs; however, excessive binding can hinder dynamic ternary complex formation. Notably, certain warheads derived from FDA-approved inhibitors retain degradation potential when incorporated into PROTACs. Comparative evaluation demonstrates that warhead modifications are frequently required to balance potency with cell permeability and ligase compatibility.

5.4 Comparative analysis of structure–activity and pharmacological profiles

Across the analyzed series, VHL- and CRBN-recruiting degraders consistently outperformed cIAP-based constructs in both enzymatic and cellular potency. Low-nanomolar EZH2 IC50 values were generally associated with pyridone-based warheads derived from tazemetostat analogues, confirming the continuing relevance of SAM-competitive pharmacophores even in dual contexts. Cellular potency varied with cell type and EZH2 dependency where hematologic models (*e.g.*, Pfeiffer, EOL-1, MV4-11) were more sensitive than solid-tumor lines, reflecting differential PRC2 reliance. Fig. 13 shows a graphical summary depicting the relationship between EZH2 inhibition and cellular cytotoxicity (both presented in IC_{50} values) on logarithmic scales. This diagram provides several analytical and interpretive advantages in evaluating PROTAC-based EZH2 degraders: it enables direct comparison of biochemical potency (target-level inhibition) with whole-cell efficacy. Compounds lying close to the diagonal line, where EZH2 IC_{50} value is almost equal to cellular IC_{50}, display good target engagement and effective translation of enzyme inhibition into antiproliferative effects. Conversely, compounds deviating indicate mechanistic issues such as incomplete inhibition or off-target cytotoxicity. Compounds with extreme values such as **E7 (13)**, which exhibits weak enzymatic potency but strong cellular activity, can be quickly recognized. Such a deviation highlights the need for further mechanistic validation. Interestingly, the inclusion of **MS8847 (84)** with its verified DC_{50} = 34 nM provides a reference point for authentic proteasome-mediated degradation. This helps distinguish true degraders from those functioning primarily as enzymatic inhibitors. VHL-engaging degraders such as **P3 (72)**, **P4 (73)**, **MS8847 (84)** cluster to the low-IC_{50} region, while CRBN- engaging degraders **U3i (44)** and **E7 (13)** show greater distribution, reflecting distinctions in cell-specific ligase expression.

These analytical observations together with the findings illustrate how ligase selection critically governs degradation efficacy in EZH2-targeted PROTACs. The verified performance of **MS8847 (84)**, with a DC_{50} of 34 nM and complete degradation within 24 h, establishes a benchmark for next-generation EZH2

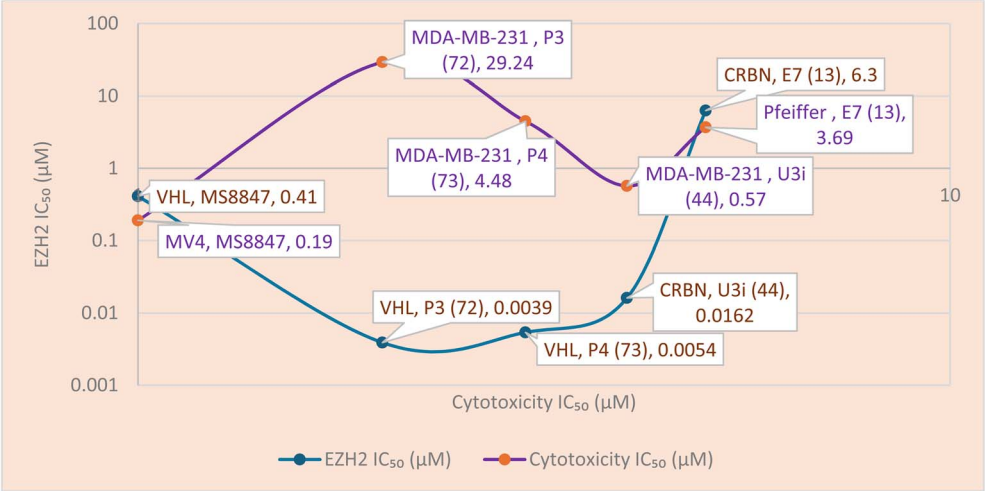

Fig. 13 Relationship between EZH2 inhibition activity (IC_{50}) and cellular cytotoxicity (IC_{50}) on logarithmic scales. All IC_{50} values were converted to same unit (μM) before plotting by dividing nanomolar values (nM) by 1000.

degraders. **P3 (72)**, **P4 (73)**, and **U3i (44)** also represent highly promising scaffolds, warranting comprehensive pharmacokinetic characterization. Future research should emphasize on quantitative degradation kinetics (DC_{50}/D_{max}) and cell-line selectivity mapping to correlate inhibition efficiency with PRC2 dependency. Ligase diversification beyond VHL/CRBN

Table 6 Pharmacological and structural highlights of the reviewed PROTAC-based EZH2 inhibitors

Cpd code	E3 ligase	EZH2 IC_{50}	Cytotoxicity IC_{50}	Ref.	Authors	Future recommendations
E7 (13)	CRBN	$EZH2^{WT}$ = 6.30 μM	Pfeiffer = 3.69 μM; prostate 0.21 μM	80	Liu *et al.*, 2021	Mechanistic follow-up required
YM281 (20)	VHL	$EZH2^{WT}$ = 0.734 μM	NCI-BL209 = 8.04 μM; raji = 7.53 μM; daudi = 5.72 μM; namalwa = 7.09 μM; JVM-2 = 6.19 μM; Jeko-1 = 7.21 μM; MINO = 4.53 μM; SU-DHL-2 = 1.49 μM; SU-DHL-4 = 3.46 μM; SU-DHL-6 = 0.95 μM	92	Tu *et al.*, 2021	Despite comparatively higher IC_{50} values, it warrants continued optimization and mechanistic exploration
YM181 (21)	VHL	$EZH2^{WT}$ = 0.502 μM	SU-DHL-2 = 3.99 μM; SU-DHL-4 = 5.09 μM; SU-DHL-6 = 2.00 μM	92	Tu *et al.*, 2021	Despite comparatively higher IC_{50} values, it warrants continued optimization and mechanistic exploration
U3i (44)	CRBN	$EZH2^{WT}$ = 16.19 nM	MDA-MB-231 = 0.57 μM; MDA-MB-468 = 0.38 μM	79	Wang *et al.*, 2022	Strong breast-cancer candidate; validate degradation kinetics
P3 (72)	VHL	$EZH2^{WT}$ = 3.90 nM	Pfeiffer = 23.09 nM; MDA-MB-231 = 29.24 μM; MDA-MB-468 = 32.27 μM; MCF-7 = 39.07 μM; T47D = >50.00 μM	99	Xiao *et al.*, 2024	Lineage-focused lymphoma lead; explore tumor-type selectivity
P4 (73)	VHL	$EZH2^{WT}$ = 5.40 nM	Pfeiffer = 2.05 μM; MDA-MB-231 = 4.48 μM; MDA-MB-468 = 1.40 μM; MCF-7 = 4.15 μM; T47D = 6.85 μM	99	Xiao *et al.*, 2024	Promising broad-spectrum degrader; merits *in vivo* PK/PD validation
MS8847 (84)	VHL	$EZH2^{WT}$ = 0.41 μM (DC_{50})	BT549 = 1.45 μM; MDA-MB-468 = 0.45 μM; MV4 = 0.19 μM	100	Velez *et al.*, 2024	Top-priority candidate for preclinical advancement; confirmed time- and concentration-dependent degradation

Table 7 Key design principles and unresolved challenges in PROTAC-based EZH2 inhibitors

Design principle	Unresolved challenges
E3 ubiquitin ligase selection	Ligase bias and off-target degradation
Linker optimization	Potential reduction in selectivity and off-target interactions
Warhead affinity	Excessive affinity can hinder ternary complex formation
Multi-cell-line evaluation	Inconsistent correlations remain

should also be considered to overcome resistance and expand tissue specificity. Based on these, Table 6 shows the pharmacological profiles of recently developed EZH2-targeted PROTACs as well as future recommendations for compounds that merit further investigation.

5.5 Limitations and unresolved challenges in PROTAC-based EZH2 degradation

Despite the advantages of PROTACs in achieving sustained and catalytic depletion of EZH2, several challenges currently limit the clinical advancement of EZH2 inhibitors.[75,101–103] A major obstacle is the unacceptable physicochemical characteristics of PROTAC-based molecules.[101,104–106] The large molecular weight, high polarity, and increased conformational flexibility associated with this class often result in poor membrane permeability and limited oral bioavailability.[107–111] In this regard, **YM281 (20)** and **MS8847 (84)** possess high molecular weights (>900 Da) and elevated polar surface areas which compromise membrane permeability and oral bioavailability.[92,100] Another key limitation relates to E3 ligase dependency and bias is that most reported EZH2 PROTACs such as **YM281 (20)**, **U3i (44)**, and **P3 (72)** rely on CRBN or von VHL ligases,[79,80,92] reflecting their favorable ligandability and expression profiles. However, heterogeneous E3 ligase expression across tumor types can lead to variable degradation efficiency, potentially restricting the therapeutic applicability of a given PROTAC.[103,111,112] Alternative ligases (MDM2 and cIAP) have underperformed due to weaker ternary complex formation or unfavorable cellular outcomes, underscoring the need for broader ligase exploration.[113] Selectivity and off-target degradation also represent important safety considerations.[40,62,114,115] While PROTACs can enhance functional selectivity by eliminating the target protein rather than merely inhibiting its catalytic activity, unintended degradation of structurally related proteins.[114,116] For EZH2 degraders, distinguishing between EZH2-selective degradation and dual EZH1/2 depletion remains challenging, particularly given the high structural homology within PRC2 components.[103,111,112] Some PROTAC-based EZH2 degraders, including **MS8847 (84)**, induce concurrent degradation of EZH1 due to the high structural homology between these paralogs within the PRC2 complex.[68] Such off-target effects may exacerbate hematological or developmental toxicities.[40,49,115] Additionally, variability in degradation efficiency across cell lines, as reported for **P3 (72)** and **P4 (73)**, underscores the need for broader biological validation beyond single-model systems. Collectively, while PROTAC-based EZH2 degraders offer a powerful strategy to overcome resistance and non-canonical EZH2 functions, addressing these challenges is essential to translate their mechanistic promise into clinically viable therapeutics. Lastly, some data shows inconsistency between the reported DC_{50} values and correlations between EZH2 degradation and antiproliferative activity across cellular models. For example, the CRBN-recruiting degrader **MS8847 (84)** achieved rapid and near-complete EZH2 depletion in several lymphoma cell lines, yet translated this effect into only modest growth inhibition in certain solid tumor models. Similarly, comparative studies on VHL-based degraders **P3 (72)** and **P4 (73)** revealed that although both compounds induced considerable EZH2 degradation, only **P4 (73)** produced consistent antiproliferative responses. In contrast, **YM281 (20)** displayed an alignment between EZH2 degradation and cytotoxicity in EZH2-dependent lymphoma cells. Table 7 summarizes the unresolved challenges *vs.* key design principles.

6 Conclusion and future perspectives

The emergence of PROTAC-based EZH2 degraders marks a transformative milestone in the evolution of epigenetic cancer therapy. Unlike conventional inhibitors that transiently block the enzymatic pocket, PROTACs enable complete and sustained inhibition of the EZH2 protein, thereby abolishing both its catalytic and non-catalytic oncogenic functions. Over the last five years, a growing portfolio of VHL-, CRBN-, and cIAP-recruiting degraders has demonstrated compelling pharmacological performance, confirming that targeted protein degradation can effectively overcome the intrinsic limitations of small-molecule inhibitors. Among these, **MS8847 (84)** represents a top-priority candidate, exhibiting potent, time- and concentration-dependent degradation ($DC_{50} = 34$ nM, maximal effect at 24 h) and robust antiproliferative activity in EOL-1 leukemia cells. Other notable examples, such as **P3 (72)**, **P4 (73)**, and **U3i (44)**, achieved selective EZH2 degradation and cytotoxic potency in multiple tumor models, underscoring the impact of E3 ligase selection and linker optimization on ternary complex formation and degradation efficiency. Collectively, these findings validate the mechanistic superiority of PROTAC degraders in delivering durable suppression of EZH2-driven oncogenic programs, including resistance to tazemetostat and $EZH2^{Y641}$ mutant variants. Despite these advances, several challenges continue to shape future research directions. Pharmacokinetic limitations (large molecular size, poor permeability), ligase dependency, and potential off-target proteome degradation remain significant barriers to clinical translation. Moreover, the cellular context of EZH2 expression and PRC2 complex dynamics requires more precise understanding. The

next generation of EZH2-targeting PROTACs are suggested to integrate novel ligase recruiters (*e.g.*, MDM2, RNF114, KEAP1) to expand tissue specificity and overcome ligase redundancy. Allosteric and covalent PROTAC designs are also encouraged to enhance selectivity and engagement kinetics. AI-guided linker design and *in silico* prediction of ternary complex stability should also be considered. Lastly, combination strategies with chromatin modulators to achieve synergistic tumor suppression is recommended. Collectively, continued medicinal chemistry innovation, coupled with structural and systems-level insights, will be essential to unlock the full therapeutic potential of this class and to translate EZH2 degraders from preclinical promise into clinical reality.

Conflicts of interest

The author declares that he has no conflict of interest.

Abbreviation

A677G	Alanine–glycine mutation at position 677 in EZH2
AKT	Protein kinase B
BRCA	Breast cancer gene
BTK	Bruton's tyrosine kinase
CDK9	Cyclin-dependent kinase 9
cIAP	Cellular inhibitor of apoptosis protein
CRBN	Cereblon
DIPEA	*N*,*N*-Diisopropylethylamine
DLBCL	Diffuse large B-cell lymphoma
DMF	*N*,*N*-Dimethylformamide
DMSO	Dimethyl sulfoxide
EDC	1-Ethyl-3-(3-dimethylaminopropyl)carbodiimide
EDCI	1-Ethyl-3-(3-dimethylaminopropyl)carbodiimide hydrochloride
EED	Embryonic ectoderm development
EOL-1	Human eosinophilic leukemia cell line
EZH1	Enhancer of zeste homolog 1
EZH2	Enhancer of zeste homolog 2
FDA	Food and drug administration
GBM	Glioblastoma
H3K27	Histone H3 lysine 27
H3K27me3	histone H3 at lysine 27
HATU	O-(7-Azabenzotriazol-1-yl)-*N*,*N*,*N*′,*N*′-tetramethyluronium hexafluorophosphate
HDAC	Histone deacetylase
HOAT	1-Hydroxy-7-azabenzotriazole
IGF-1R	Insulin-like growth factor 1 receptor
MAPK	Mitogen-activated protein kinase
MEK	MAPK/ERK kinase
NAE	NEDD8-activating enzyme
nM	Nanomole
ORR	Overall response rate
PARP	Poly ADP-ribose polymerase
PD	Pharmacodynamics
PDB	Protein data bank
PI3K	Phosphoinositide 3-kinase
PI3KCA	Phosphatidylinositol-4,5-bisphosphate 3-kinase catalytic subunit alpha
PK	Pharmacokinetic
PRC2	Polycomb repressive complex 2
PROTAC	Proteolysis-targeting chimera
RB1/E2F	Retinoblastoma protein/e2f transcription factor
SAHA	Suberoylanilide hydroxamic acid (Vorinostat)
SAM	S-adenosylmethionine
SAR	Structure–activity relationship
SET	Su(var)3–9, enhancer-of-zeste, trithorax
SMARCB1	SWI/SNF Related, matrix associated, actin dependent regulator of chromatin, subfamily b, member 1
SN2	Bimolecular nucleophilic substitution
SU-DHL-6	Diffuse large b-cell lymphoma cell line
SUZ12	Suppressor of zeste 12 homolog
TNBC	Triple-negative breast cancer
TRAEs	Treatment-related adverse events
VHL	von Hippel-Lindau

Data availability

No primary research results, software or code have been included and no new data were generated or analysed as part of this review.

Supplementary information (SI) is available. See DOI: https://doi.org/10.1039/d5ra08746e.

Acknowledgements

While preparing the initial draft of this manuscript, ChatGPT was utilized for brainstorming, structuring ideas, and drafting some paragraphs. However, the author took full responsibility for analyzing, editing, and verifying the final data, and ensuring the accuracy of the research contents.

References

1 P. Kumari, S. Garg, A. K. Arya, J. Kaur, N. K. Sachdeva, U. N. Saikia, D. Dahiya, S. K. Bhadada and S. D. Rao, *Expert Opin. Ther. Targets*, 2025, **29**, 159–169.
2 J. Xia, J. Li, L. Tian, X. Ren, C. Liu and C. Liang, *J. Med. Chem.*, 2022, **65**, 7016–7043.
3 X. Tian, K. Newlander, L. LaFrance, J. Mack, J. Brackley, C. McHugh, Y. He, N. Johnson, M. Truong, M. B. Pappalardi, M. T. McCabe and S. D. Knight, *Bioorg. Med. Chem. Lett.*, 2025, **127**, 130291.
4 P. Goleij, M. M. Heidari, M. A. K. Tabari, M. Hadipour, A. Rezaee, A. Javan, P. M. Sanaye, D. S. Larsen, M. Daglia and H. Khan, *Funct. Integr. Genomics*, 2025, **25**, 53.
5 Z. Chen, Z. Yao, M. Wu, Y. Wu, J. Zhang, Z. Liao, J. Qian, J. Wei, L. Song, L. Yu, J. Wen, Z. Zhou, Y. Wei, Y. Yao, Z. Ma, P. Liu, S. Agarwal, Y. Li, L. Xue and D. Wang, *J. Orthop. Transl.*, 2025, **55**, 309–322.

6 Y. Guo, R. Cheng, Y. Wang, M. E. Gonzalez, H. Zhang, Y. Liu, C. G. Kleer and L. Xue, *eBioMedicine*, 2024, **100**, 104972.
7 P. Kaur, E. Shankar and S. Gupta, *Cancer Lett.*, 2024, **586**, 216706.
8 R. G. Kruger, A. P. Graves and M. T. McCabe, in *Polycomb Group Proteins*, Elsevier, 2017, pp. 259–288.
9 Y. Zhang, J. Shen, J. Li, Z. Wang, Y. Wang, Y. Zhu, S. Ding, Y. Zhou, Y. Chen and J. Liu, *New J. Chem.*, 2023, **47**, 21318–21331.
10 B. Lu, X. Shen, L. Zhang, D. Liu, C. Zhang, J. Cao, R. Shen, J. Zhang, D. Wang, H. Wan, Z. Xu, M.-H. Ho, M. Zhang, L. Zhang, F. He and W. Tao, *ACS Med. Chem. Lett.*, 2018, **9**, 98–102.
11 L. Wei, D. Mei, S. Hu and S. Du, *Future Med. Chem.*, 2024, **16**, 1561–1582.
12 A. Mahajan, G. Panzade, T. Bhuniya, P. Das, B. Bhattacharjee, S. Das, A. Chowdhury, K. Chakraborty, S. Guha, A. Samant, A. Dey, S. Ghosh and C. Probl, *Cancer*, 2025, **54**, 101172.
13 V. Mathur, M. Jha, I. Zai, M. Mahajan, S. Nazar, S. Ali, A. Ilyas, S. Tanweer, J. Ali and O. Alam, *Med. Drug Discov.*, 2025, **27**, 100221.
14 N. J. van Eck and L. Waltman, *Scientometrics*, 2010, **84**, 523–538.
15 M. S. Wang, J. Sussman, J. A. Xu, R. Patel, O. Elghawy and P. Rawla, *Life*, 2024, **14**, 1645.
16 A. M. Malebari, H. E. A. Ahmed, S. K. Ihmaid, A. M. Omar, Y. A. Muhammad, S. S. Althagfan, N. Aljuhani, A. A. A. A. El-Sayed, A. H. Halawa, H. M. El-Tahir, S. A. Turkistani, M. Almaghrabi, A. K. B. Aljohani, A. M. El-Agrody and H. S. Abulkhair, *Bioorg. Chem.*, 2023, **130**, 106255.
17 E. M. Husseiny, H. S. Abulkhair, N. M. El-Dydamony and K. E. Anwer, *Bioorg. Chem.*, 2023, 106397.
18 A. A. Al-Karmalawy, M. Rashed, M. Sharaky, H. S. Abulkhair, M. M. Hammouda, H. O. Tawfik and M. A. Shaldam, *Eur. J. Med. Chem.*, 2023, **259**, 115661.
19 H. Wu, H. Zeng, A. Dong, F. Li, H. He, G. Senisterra, A. Seitova, S. Duan, P. J. Brown, M. Vedadi, C. H. Arrowsmith and M. Schapira, *PLoS One*, 2013, **8**, e83737.
20 T.-P. Liu, H.-L. Lo, L.-S. Wei, H. Hao-yun Hsiao and P.-M. Yang, *Anticancer. Drugs*, 2015, **26**, 139–147.
21 M. Wassef, A. Luscan, S. Aflaki, D. Zielinski, P. W. T. C. Jansen, H. I. Baymaz, A. Battistella, C. Kersouani, N. Servant, M. R. Wallace, P. Romero, O. Kosmider, P.-A. Just, M. Hivelin, S. Jacques, A. Vincent-Salomon, M. Vermeulen, M. Vidaud, E. Pasmant and R. Margueron, *Proc. Natl. Acad. Sci. U. S. A.*, 2019, **116**, 6075–6080.
22 R. Qin, B. Ma, S. Mou, M. Yuan, J. Xing, J. Shen, S. Ding, Y. Chen and J. Liu, *Mol. Divers.*, DOI: 10.1007/s11030-025-11272-w.
23 Y. Liu and Q. Yang, *Med. Oncol.*, 2023, **40**, 167.
24 A. A. Sahasrabuddhe, X. Chen, F. Chung, T. Velusamy, M. S. Lim and K. S. J. Elenitoba-Johnson, *Oncogene*, 2015, **34**, 445–454.
25 T. J. Wigle, S. K. Knutson, L. Jin, K. W. Kuntz, R. M. Pollock, V. M. Richon, R. A. Copeland and M. P. Scott, *FEBS Lett.*, 2011, **585**, 3011–3014.
26 M. T. McCabe, A. P. Graves, G. Ganji, E. Diaz, W. S. Halsey, Y. Jiang, K. N. Smitheman, H. M. Ott, M. B. Pappalardi, K. E. Allen, S. B. Chen, A. Della Pietra, E. Dul, A. M. Hughes, S. A. Gilbert, S. H. Thrall, P. J. Tummino, R. G. Kruger, M. Brandt, B. Schwartz and C. L. Creasy, *Proc. Natl. Acad. Sci. U. S. A.*, 2012, **109**, 2989–2994.
27 C. R. Majer, L. Jin, M. P. Scott, S. K. Knutson, K. W. Kuntz, H. Keilhack, J. J. Smith, M. P. Moyer, V. M. Richon, R. A. Copeland and T. J. Wigle, *FEBS Lett.*, 2012, **586**, 3448–3451.
28 D. B. Yap, J. Chu, T. Berg, M. Schapira, S.-W. G. Cheng, A. Moradian, R. D. Morin, A. J. Mungall, B. Meissner, M. Boyle, V. E. Marquez, M. A. Marra, R. D. Gascoyne, R. K. Humphries, C. H. Arrowsmith, G. B. Morin and S. A. J. R. Aparicio, *Blood*, 2011, **117**, 2451–2459.
29 S. N. Chi, J. S. Yi, P. M. Williams, S. Roy-Chowdhuri, D. R. Patton, B. D. Coffey, J. M. Reid, J. Piao, L. Saguilig, T. A. Alonzo, S. L. Berg, N. C. Ramirez, A. Jaju, J. C. Mhlanga, E. Fox, D. S. Hawkins, M. M. Mooney, N. Takebe, J. V Tricoli, K. A. Janeway, N. L. Seibel and D. W. Parsons, *JNCI J. Natl. Cancer Inst.*, 2023, **115**, 1355–1363.
30 M. Sabour-Takanlou, L. Sabour-Takanlou and C. Biray-Avci, *Clin. Genet.*, 2024, **106**, 377–385.
31 K. Kato, *Int. J. Hematol.*, 2022, **116**, 819–820.
32 M. S. Gilardini Montani, R. Benedetti and M. Cirone, *Molecules*, 2024, **29**, 5817.
33 FDA, Approves tazemetostat for advanced epithelioid sarcoma, https://www.fda.gov/drugs/resources-information-approved-drugs/fda-approves-tazemetostat-advanced-epithelioid-sarcoma, accessed 3 November 2025.
34 R. Straining and W. Eighmy, *PharmD, J. Adv. Pract. Oncol.*, 2022, **13**, 158–163.
35 D. Wu, X. Zeng, Y. Zhao, M. Qin and P. Gong, *Bioorg. Med. Chem.*, 2024, **105**, 117725.
36 X. Chen, C. Wang, D. Lu, H. Luo, S. Li, F. Yin, Z. Luo, N. Cui, L. Kong and X. Wang, *Bioorg. Med. Chem.*, 2023, **91**, 117386.
37 M. Orleni and J. H. Beumer, *Cancer Chemother. Pharmacol.*, 2024, **93**, 509–517.
38 E. Julia and G. Salles, *Futur. Oncol.*, 2021, **17**, 2127–2140.
39 S. K. Knutson, T. J. Wigle, N. M. Warholic, C. J. Sneeringer, C. J. Allain, C. R. Klaus, J. D. Sacks, A. Raimondi, C. R. Majer, J. Song, M. P. Scott, L. Jin, J. J. Smith, E. J. Olhava, R. Chesworth, M. P. Moyer, V. M. Richon, R. A. Copeland, H. Keilhack, R. M. Pollock and K. W. Kuntz, *Nat. Chem. Biol.*, 2012, **8**, 890–896.
40 L. Yu, M. Xia, Y. Wang, Z. Yan, L. Zhang and S. Li, *Med. Chem. Res.*, 2023, **32**, 1589–1604.
41 EZH2 Selective Inhibitors, https://www.selleckchem.com/subunits/EZH2_EZH1/2_selpan.html, accessed 12 October 2025.
42 Dose Escalation and Expansion Study of HM97662 in Advanced or Metastatic Solid Tumors.

43 B. Zhou, X. Liang, H. Mei, S. Qi, Z. Jiang, A. Wang, F. Zou, Q. Liu, J. Liu, W. Wang, C. Hu, Y. Chen, Z. Wang, B. Wang, L. Wang, J. Liu and Q. Liu, *J. Med. Chem.*, 2021, **64**, 15170–15188.
44 J. Byun, S. H. Jung, Y.-Y. Kim, M. Lee, G. Lee, H. Moon, J. Park, S. Yeong, Y. G. Ahn, Y. H. Kim and K. H. Suh, 2021.
45 S. Makita and K. Tobinai, *Lancet Oncol.*, 2018, **19**, 586–587.
46 M. Bratkowski, X. Yang and X. Liu, *Sci. Rep.*, 2018, **8**, 9092.
47 D. S. BIOVIA, 2017, R2, https://www.materials-studio.com/products/collaborative-science/biovia-discovery-studio/.
48 S. Ihmaid, H. E. A. Ahmed, A. Al-Sheikh Ali, Y. E. Sherif, H. M. Tarazi, S. M. Riyadh, M. F. Zayed, H. S. Abulkhair and H. S. Rateb, *Bioorg. Chem.*, 2017, **72**, 234–247.
49 A. M. Malebari, M. A. M. Ali, A. Musa, M. E. A. Zaki, S. M. Gomha, M. A. Soliman, M. A. Abdelgawad, D. G. Thomas Parambi, M. R. Aouad, H. S. Abulkhair and H. E. A. Ahmed, *RSC Adv.*, 2025, **15**, 47601–47618.
50 H. Abul-Khair, S. Elmeligie, A. Bayoumi, A. Ghiaty, A. El-Morsy and M. H. Hassan, *J. Heterocycl. Chem.*, 2013, **50**, 1202–1208.
51 A. Feoli, M. Viviano, A. Cipriano, C. Milite, S. Castellano and G. Sbardella, *RSC Chem. Biol.*, 2022, **3**, 359–406.
52 M. Kotev, P. Manuel-Manresa, E. Hernando, V. Soto-Cerrato, M. Orozco, R. Quesada, R. Pérez-Tomás and V. Guallar, *J. Chem. Inf. Model.*, 2017, **57**, 2089–2098.
53 M. Xu, C. Xu, R. Wang, Q. Tang, Q. Zhou, W. Wu, X. Wan, H. Mo, J. Pan and S. Wang, *Genes Dis.*, 2025, **12**, 101313.
54 S. Kikuchi, Y. Nabe, R. Horaguchi, T. Minemura, J. Murakami, A. Noguchi, K. Takagi, Y. Kamihara, A. Wada, T. Fujihira and T. Sato, *Int. Cancer Conf. J.*, 2024, **13**, 488–492.
55 A Study of Valemetostat Tosylate in Combination With DXd ADCs in Subjects With Solid Tumors.
56 E. Y. Rosen, N. N. Shukla and J. L. Glade Bender, *JNCI J. Natl. Cancer Inst.*, 2023, **115**, 1246–1248.
57 UroToday, EZH2 Inhibition for Prostate Cancer; It's Taken Awhile, but We Just May Be onto Something Here, https://www.urotoday.com/clinical-trials/from-the-editor/158604-ezh2-inhibition-for-prostate-cancer-it-s-taken-awhile-but-we-just-may-be-onto-something-here.html, accessed 12 October 2025.
58 NCI, Targeted Treatment for Metastatic Prostate Cancer, The PREDICT Trial (PREDICT), https://clinicaltrials.gov/study/NCT06632977, accessed 12 October 2025.
59 Mevrometostat Treatment of Relapsed/Refractory SCLC, Castration Resistant Prostate Cancer, and Follicular Lymphoma.
60 S. H. Jung, J. Byun, Y.-Y. Kim, S. Y. Han, M. Lee, G. Lee, J. Park, Y. G. Ahn, Y. H. Kim, K. H. Suh and Y. Koh, *Blood*, 2023, **142**, 7134.
61 Y. Jeong, S. B. Kim, C.-E. Yang, M. S. Yu, W.-S. Choi, Y. Jeon and J.-Y. Lim, *Front. Oncol.*, 2023, **13**, DOI: 10.3389/fonc.2023.1252658.
62 Selleckchem, Tazemetostat (EPZ-6438), https://www.selleckchem.com/products/epz-6438.html#:~:text=TazemetostatEPZ-6438CE74389isapotentCandselective,andE4C500-foldselectivityrelativeto14otherHMTs, accessed 3 November 2025.
63 M. T. Khayat, H. E. A. Ahmed, A. M. Omar, Y. A. Muhammad, K. A. Mohammad, A. M. Malebari, A. N. Khayyat, A. H. Halawa, H. S. Abulkhair, A. A. Al-Karmalawy, M. Almaghrabi, M. Alharbi, A. S. Aljahdali and A. M. El-Agrody, *J. Biomol. Struct. Dyn.*, 2023, **41**, 15243–15261.
64 Z. Wang, Y. Su, D. Zhuang and T. Lan, *J. Mol. Neurosci.*, 2021, **71**, 556–564.
65 Z. Zhao, X. Chen, H. Pang, Y. Shi and H. Sun, *PeerJ*, 2025, **13**, e18871.
66 Q. Liu, M. Luo, M. Gao, B. Yang, X. Liu and G. Liang, *Ther. Innov. Regul. Sci.*, 2026, **60**, 92–104.
67 American Society of Clinical Oncology, ASCO GU 2025: Mevrometostat (PF-06821497), an EZH2 Inhibitor, in *Combination with Enzalutamide in Patients with mCRPC: A Randomized Dose-Expansion Study*, https://www.urotoday.com/conference-highlights/asco-gu-2025/asco-gu-2025-prostate-cancer/158201-asco-gu-2025-mevrometostat-pf-06821497-an-ezh2-inhibitor-in-combination-with-enzalutamide-in-patients-with-mcrpc-a-randomized-dose-expansion-study.html, accessed 12 October 2025.
68 M. Bisserier and N. Wajapeyee, *Blood*, 2018, **131**, 2125–2137.
69 Y. Kazansky, D. Cameron, H. S. Mueller, P. Demarest, N. Zaffaroni, N. Arrighetti, V. Zuco, Y. Kuwahara, R. Somwar, M. Ladanyi, R. Qu, E. de Stanchina, F. S. Dela Cruz, A. L. Kung, M. M. Gounder and A. Kentsis, *Cancer Discov.*, 2024, **14**, 965–981.
70 Y. Chen, H. Zhu, Y. Luo, S. Tong and Y. Liu, *Biomed. Pharmacother.*, 2024, **175**, 116624.
71 M. Y. He and R. Kridel, *Leukemia*, 2021, **35**, 2151–2165.
72 E. Riquelme, C. Behrens, H. Y. Lin, G. Simon, V. Papadimitrakopoulou, J. Izzo, C. Moran, N. Kalhor, J. J. Lee, J. D. Minna and I. I. Wistuba, *Cancer Res.*, 2016, **76**, 675–685.
73 J. Yang, J. Xu, W. Wang, B. Zhang, X. Yu and S. Shi, *Signal Transduct. Target. Ther.*, 2023, **8**, 210.
74 J. Desantis, A. Mammoli, M. Eleuteri, A. Coletti, F. Croci, A. Macchiarulo and L. Goracci, *RSC Adv.*, 2022, **12**, 21968–21977.
75 U. Patel, J. P. Smalley and J. T. Hodgkinson, *RSC Chem. Biol.*, 2023, **4**, 623–634.
76 C. Sharma, D. Donu, A. M. Curry, E. Barton and Y. Cen, *RSC Adv.*, 2023, **13**, 11771–11781.
77 Q. Zhang, X. Chen, X. Hu, X. Duan, G. Wan, L. Li, Q. Feng, Y. Zhang, N. Wang and L. Yu, *Biomed. Pharmacother.*, 2022, **147**, 112617.
78 Z. Guo, Y. Sun, L. Liang, W. Lu, B. Luo, Z. Wu, B. Huo, Y. Hu, P. Huang, Q. Wu and S. Wen, *J. Med. Chem.*, 2022, **65**, 6573–6592.
79 C. Wang, X. Chen, X. Liu, D. Lu, S. Li, L. Qu, F. Yin, H. Luo, Y. Zhang, Z. Luo, N. Cui, L. Kong and X. Wang, *Eur. J. Med. Chem.*, 2022, **238**, 114462.

80 Z. Liu, X. Hu, Q. Wang, X. Wu, Q. Zhang, W. Wei, X. Su, H. He, S. Zhou, R. Hu, T. Ye, Y. Zhu, N. Wang and L. Yu, *J. Med. Chem.*, 2021, **64**, 2829–2848.
81 G. Zhong, X. Chang, W. Xie and X. Zhou, *Signal Transduct. Target. Ther.*, 2024, **9**, 308.
82 N. A. Zografou-Barredo, A. J. Hallatt, J. Goujon-Ricci and C. Cano, *Bioorg. Med. Chem.*, 2023, **88–89**, 117334.
83 M. Cai, F. Ma, C. Hu, H. Li, F. Cao, Y. Li, J. Dong and J.-J. Qin, *Bioorg. Med. Chem.*, 2023, **90**, 117352.
84 H. S. Abulkhair, *Arch. Pharm. (Weinheim).*, 2025, **358**, e2400802.
85 H. S. Abulkhair and K. El-Adl, *Arch. Pharm. (Weinheim).*, 2025, **358**, e2500033.
86 H. S. Abulkhair, *Bioorganic Med. Chem.*, 2025, **130**, 118389.
87 H. S. Abulkhair, *Future Med. Chem.*, 2025, **17**, 3025–3040.
88 M. Salem, K. El-Adl, A. El-morsy and H. S. Abulkhair, *RSC Adv.*, 2025, **15**, 32778–32795.
89 H. S. Abulkhair, *Bioorg. Chem.*, 2026, **168**, 109305.
90 H. S. Abulkhair, *Egypt. J. Chem.*, 2025, **68**, 159–174.
91 R. Cao, J. Ni, X. Zhang, M. Qi, Z. Zhang, Z. Liu and G. Chen, *Bioorg. Chem.*, 2025, **154**, 108070.
92 Y. Tu, Y. Sun, S. Qiao, Y. Luo, P. Liu, Z.-X. Jiang, Y. Hu, Z. Wang, P. Huang and S. Wen, *J. Med. Chem.*, 2021, **64**, 10167–10184.
93 H. Xie, W. Xu, J. Liang, Y. Liu, C. Zhuo, X. Zou, W. Luo, J. Xiao, Y. Lin, L. Chen and H. Li, *Bioorg. Chem.*, 2023, **140**, 106762.
94 A. Urbina, A. J. Hallatt, J. Robertson and A. Ciulli, *Expert Opin. Ther. Pat.*, 2025, **35**, 197–238.
95 C. Wang, Y. Zhang, J. Wang and D. Xing, *Eur. J. Med. Chem.*, 2022, **227**, 113906.
96 Y. Itoh, M. Ishikawa, M. Naito and Y. Hashimoto, *J. Am. Chem. Soc.*, 2010, **132**, 5820–5826.
97 D. Mi, Y. Li, H. Gu, Y. Li and Y. Chen, *Eur. J. Med. Chem.*, 2023, **256**, 115444.
98 A. Bricelj, C. Steinebach, R. Kuchta, M. Gütschow and I. Sosič, *Front. Chem.*, 2021, **9**, DOI: 10.3389/fchem.2021.707317.
99 B. Xiao, Z. Shi, J. Liu, Q. Huang, K. Shu, F. Liu, C. Zhi, D. Zhang, L. Wu, S. Yang, X. Zeng, T. Fan, Z. Liu and Y. Jiang, *Bioorg. Chem.*, 2024, **143**, 107078.
100 J. Velez, B. Dale, K.-S. Park, H. Ü. Kaniskan, X. Yu and J. Jin, *Eur. J. Med. Chem.*, 2024, **267**, 116154.
101 S. Zeng, Y. Ye, H. Xia, J. Min, J. Xu, Z. Wang, Y. Pan, X. Zhou and W. Huang, *Eur. J. Med. Chem.*, 2023, **261**, 115793.
102 W. Dai, X. Qiao, Y. Fang, R. Guo, P. Bai, S. Liu, T. Li, Y. Jiang, S. Wei, Z. Na, X. Xiao and D. Li, *Signal Transduct. Target. Ther.*, 2024, **9**, 332.
103 A. A. Al-Karmalawy, M. E. Eissa, N. A. Ashour, T. A. Yousef, A. O. Al Khatib and S. S. Hawas, *RSC Adv.*, 2025, **15**, 36441–36471.
104 C. A. Lipinski, F. Lombardo, B. W. Dominy and P. J. Feeney, *Adv. Drug Deliv. Rev.*, 1997, **23**, 3–25.
105 A. Musa, S. K. Ihmaid, D. L. Hughes, M. A. Said, H. S. Abulkhair, A. H. El-Ghorab, M. A. Abdelgawad, K. Shalaby, M. E. Shaker, K. S. Alharbi, N. H. Alotaibi, D. L. Kays, L. J. Taylor, D. G. T. Parambi, S. I. Alzarea, A. A. Al-Karmalawy, H. E. A. Ahmed and A. M. El-Agrody, *J. Biomol. Struct. Dyn.*, 2023, **41**, 12411–12425.
106 A. Turky, F. F. Sherbiny, A. H. Bayoumi, H. E. A. Ahmed and H. S. Abulkhair, *Arch. Pharm. (Weinheim)*, 2020, **353**, 2000170.
107 B. J. Boyd, C. A. S. Bergström, Z. Vinarov, M. Kuentz, J. Brouwers, P. Augustijns, M. Brandl, A. Bernkop-Schnürch, N. Shrestha, V. Préat, A. Müllertz, A. Bauer-Brandl and V. Jannin, *Eur. J. Pharm. Sci.*, 2019, **137**, 104967.
108 S. Wang, G. König, H.-J. Roth, M. Fouché, S. Rodde and S. Riniker, *J. Med. Chem.*, 2021, **64**, 12761–12773.
109 X. Xu, J. Chen, G. Wang, X. Zhang, Q. Li, X. Zhou, F. Guo and M. Li, *Bioorg. Med. Chem. Lett.*, 2024, **97**, 129558.
110 E. M. Othman, E. A. Fayed, E. M. Husseiny and H. S. Abulkhair, *New J. Chem.*, 2022, **46**, 12206–12216.
111 H. Pei, Y. Peng, Q. Zhao and Y. Chen, *RSC Adv.*, 2019, **9**, 16967–16976.
112 C. Sampson, Q. Wang, W. Otkur, H. Zhao, Y. Lu, X. Liu and H. Piao, *Clin. Transl. Med.*, 2023, **13**, DOI: 10.1002/ctm2.1204.
113 R. P. Wurz, H. Rui, K. Dellamaggiore, S. Ghimire-Rijal, K. Choi, K. Smither, A. Amegadzie, N. Chen, X. Li, A. Banerjee, Q. Chen, D. Mohl and A. Vaish, *Nat. Commun.*, 2023, **14**, 4177.
114 J. Yang, Y. Zhang, M. Zhang, D. Xing and C. Wang, *Mater. Today Adv.*, 2025, **28**, 100644.
115 G. Fan, S. Chen, Q. Zhang, N. Yu, Z. Shen, Z. Liu, W. Guo, Z. Tang, J. Yang and M. Liu, *MedComm*, 2025, **6**, e70401.
116 Y. Wang, X. Jiang, F. Feng, W. Liu and H. Sun, *Acta Pharm. Sin. B*, 2020, **10**, 207–238.